Staphylococcus aureus small-colony variants exhibit genotype specific hyperinflammation

Qing Tang[1], Mimi R. Precit[1], Maureen K. Thomason[1], Fariha Ahmed-Qadri[1], Adelle P. McFarland[1], Daniel J. Wolter[2, 3], Lucas R. Hoffman[1, 2, 3], Joshua J. Woodward[1, 4, *]

[1]Department of Microbiology, University of Washington, Seattle, WA 98105, USA
[2]Department of Pediatrics, University of Washington, Seattle, WA 98105, USA
[3]Pulmonary and Sleep Medicine, Seattle Children's Hospital, Seattle, WA 98105, USA
[4]Lead Contact
*Correspondence: jjwoodwa@uw.edu

SUMMARY

Staphylococcus aureus small colony variants (SCVs) cause a variety of persistent, antibiotic resistant infections. Respiratory infection with thymidine-dependent SCVs is common among children with cystic fibrosis and is associated with worse respiratory outcomes, although the underlying pathophysiological mechanisms remain to be defined. Here, we characterized normal colony (NC) *S. aureus* and two phenotypically distinct SCVs, hemin-dependent (HD-SCV) and thymidine-dependent (TD-SCV), for their capacities to affect host responses. Among these, TD-SCVs produced elevated levels of c-di-AMP in a thymidine-dependent fashion. TD-SCVs elicited increased IFN-I production in a STING-dependent and cGAS-independent manner during macrophage infection. However, murine lung infection with TD-SCVs revealed both STING-dependent increases in G-CSF and STING-independent elevation of CCL3, leading to higher airway neutrophil infiltration and activation, which were reduced by pharmacological blockade of CCL3 signaling. Our results suggest the elevated inflammatory capacity of TD-SCVs may contribute to their pathogenesis, and that targeting CCL3-mediated inflammation may improve outcomes.

INTRODUCTION

Antibiotic therapy can drive the emergence of *Staphylococcus aureus* isolates harboring mutations in fundamental metabolic pathways. Examples of such mutants include small colony variants (SCVs), which exhibit slow *in vitro* growth phenotypes and are associated with antibiotic-refractory, chronic infections, including osteomyelitis, endocarditis, and chronic wound infections. Aminoglycoside therapy, which requires a proton motive force for efficient drug uptake into the bacterial cell, results in the clinical emergence of SCV isolates auxotrophic for menadione and hemin that are deficient for respiration (Bates et al., 2003). Inactivating mutations in the thymidylate synthase encoding gene *thyA* results in thymidine dependent-SCVs (TD-SCVs), which emerge following administration of the tetrahydrofolate synthesis pathway inhibitor trimethoprim-sulfamethoxazole (TMP-SMX) (Kahl et al., 2003; Kriegeskorte et al., 2015). ThyA

uses tetrahydrofolate as a co-factor, and inactivation of ThyA leads to dependence on extracellular thymidine sources for growth, as well as TMP-SMX resistance (Chatterjee et al., 2008; Zander et al., 2008). As such, SCV related infections can persist for many years, and eradication is difficult.

S. aureus SCVs have been identified in a variety of chronic infections but are prevalent in the respiratory tract of people with cystic fibrosis (CF), an autosomal recessive genetic disorder characterized by chronic polymicrobial lung infections (Proctor et al., 2006; Yagci et al., 2013). Inflammation-induced airway tissue damage is a significant determinant of morbidity and mortality in people with CF and is associated with neutrophils and other inflammatory mediators responding to microbial presence. *S. aureus* is the bacterium detected most frequently from respiratory secretions of children with CF (Registry, 2018), and infection can persist for years despite seemingly appropriate antibiotic treatment. Several studies have revealed a high prevalence of *S. aureus* SCVs among CF patients (Kahl et al., 2003; Proctor et al., 2006; Wolter et al., 2019; Yagci et al., 2013). While preliminary clinical analysis revealed an association between SCVs and declining lung function without considering SCV subtype, a recent two-year multi-center longitudinal study among 200 children with CF reported that infection with TD-SCVs is associated with reduced lung function and increased risk of respiratory exacerbations compared to either normal colony *S. aureus* or other SCVs subtypes (Wolter et al., 2013, 2019). However, the mechanisms by which TD-SCV infection contributes to more severe respiratory outcomes are not understood. Studies that characterize the physiological and pathogenic traits of *S. aureus* SCVs are warranted as they may provide insight to achieving bacterial eradication and improved health outcomes for CF patients, among other infections.

Cyclic dinucleotides of both bacterial and host origin play key roles in mediating host immune responses to infection. STING detection of bacterial cyclic dinucleotides (c-di-AMP, c-di-GMP and 3′3′-cGAMP), or eukaryotic 2′3′-cGAMP, which is synthesized by cGAS in response to host or pathogen DNA, is an important strategy for innate immune recognition of pathogens (Burdette et al., 2011; Ishikawa and Barber, 2008; Sun et al., 2013; Wu et al., 2013; Zhang et al., 2013). Upon binding to cyclic di-nucleotides, STING recruits the kinase TBK1 through its C-terminal tail (CTT) domain, resulting in IRF3 phosphorylation and translocation to the nucleus, where IRF3 then mediates transcription of IFN-β and other coregulated genes (Burdette et al., 2011). While induction of IFN-β is the major outcome of STING activation in mammals, STING is able to induce NF-κB, MAP kinase, and STAT6 activation (Abe and Barber, 2014; Balka et al., 2020; Chen et al., 2011; McWhirter et al., 2009). STING has also been reported to promote autophagy and NLRP3 inflammasome activation independent of IFN-β (Gaidt et al., 2017; Gui et al., 2019; Zhang et al., 2020). Given the diverse mechanisms of STING signaling and expression in distinct organs (Ishikawa and Barber, 2008), this signaling pathway has emerged as a key mediator of protective host inflammation during infection in a variety of contexts.

In this study, we show that compared to normal colony (NC) *S. aureus* and a respiration deficient SCV, TD-SCVs produce elevated levels of c-di-AMP, an essential osmoregulator of bacteria. The production of c-di-AMP by TD-SCVs was dependent upon extracellular thymidine availability. We show that survival of TD-SCVs is compromised in concentrations of NaCl representative of those achieved with a common CF treatment, inhaled hypertonic saline. TD-SCVs elicited increased type I IFN in a STING-dependent manner during bone marrow derived macrophage infection *ex vivo*. In contrast, TD-SCVs elicited STING-dependent airway neutrophil activation in a murine lung infection model, but without significant type I IFN induction. Instead, our results suggest that this TD-SCV-induced airway neutrophil activation was mediated by CCL3 and G-CSF. Notably, we revealed that the production of the G-CSF is controlled by STING upon c-di-AMP stimulation or TD-SCV infection. The neutrophil attractant CCL3, which is uniquely elevated during TD-SCV lung infection, is partially controlled by STING and is critical for airway neutrophil infiltration upon TD-SCV infection. Pharmacological blockade of CCL3 signaling resulted in diminished neutrophil recruitment by TD-SCVs. Collectively, our studies provide evidence of TD-SCV elevated lung inflammation and neutrophil recruitment, providing a potential mechanistic explanation for TD-SCV associated lung function decline among people with CF, as well as providing a promising new therapeutic target to improve outcomes.

RESULTS

Δ*thyA* mutant exhibits diminished survival in cells and *in vivo*

S. aureus SCVs of various subtypes have been linked to chronic, antibiotic resistant infection and correlated with advanced lung function decline among CF patients (Wolter et al., 2013). Of these subtypes, respiratory infection with TD-SCVs is independently associated with reduced lung function and increased risk of respiratory exacerbations in pediatric CF patients (Wolter et al., 2013, 2019). To investigate the mechanisms behind these observations, we generated strains with deletions in the thymidylate synthase gene *thyA* and the porphobilinogen synthase gene *hemB* in *S. aureus* Newman. These genes were selected based upon previous literature establishing that their deletion in laboratory strains results in thymidine-deficient and electron transport chain-deficient SCVs, respectively, and that SCVs with the resulting phenotypes are recovered from clinical specimens (Bates et al., 2003; Chatterjee et al., 2008). The *hemB* gene was selected as an SCV control to compare to the Δ*thyA* strain because, although hemin-deficient SCVs exhibit slow growth rates and antibiotic resistance, they are not known to be associated with faster pulmonary decline in CF patients (Wolter et al., 2019). Thus, we hypothesized that differences between these strains could reveal mechanisms by which TD-SCVs uniquely contribute to worse respiratory outcomes.

We first confirmed that the growth of Δ*thyA* and Δ*hemB* on indicator media was each complemented by supplementation of exogenous thymidine or hemin, respectively (**Figure 1A**).

To investigate the strains' survival and signaling response in phagocytes, we used an immortalized murine bone marrow derived macrophage (iBMDM) model. iBMDMs were infected with either NC, Δ*thyA*, or Δ*hemB S. aureus* Newman strain, and intracellular bacterial survival and induction of host cell death were assessed. While there was a decline in intracellular recovery of colony forming units (CFU) for all strains over 6 hours post infection (hpi), this decline was most marked for the Δ*thyA* strain (**Figure 1B**). Similarly, all strains generated comparably low levels of macrophage toxicity at 4 hpi, as assessed by LDH release (**Figure 1C**). However, murine immune cells lack the receptors for *S. aureus* toxins LukSF and LukAB (Alonzo and Torres, 2014). Therefore, the human monocyte cell line THP-1 was used to further characterize the survival and cell toxicity of Δ*thyA* in human cells. Consistent with the observation in iBMDMs, Δ*thyA* exhibited greater decline in survival and similar cell toxicity compared with both Newman and Δ*hemB* in THP-1 cells (**Figure 1D and E**).

To determine whether these intracellular infection phenotypes were reflected during *in vivo* infections, we monitored the bacterial recovery of SCVs from murine lungs after intranasally infecting wild-type mice with either the Δ*thyA* or Δ*hemB* strains, respectively. As for both iBMDM and THP-1 cells, Δ*thyA* exhibited significantly reduced survival *in vivo* relative to Δ*hemB* from 6 hpi, and most of the inoculum was cleared by the host at 72 hpi (**Figure 1F**). Given the diminished *in vivo* virulence of TD-SCVs observed by us and others (Kriegeskorte et al., 2014), these findings suggest that the association with worse CF clinical outcomes of TD-SCV isolates is not attributable either to elevated bacterial burden or differential cellular cytotoxicity during infection compared with other *S. aureus*.

Δ*thyA* induces higher inflammatory gene expression in macrophages

Given these initial findings, we hypothesized that TD-SCVs may exhibit elevated proinflammatory capacity that promotes pathological tissue damage leading to worse CF clinical outcomes. To investigate the inflammatory capacity of TD-SCVs, transcriptional profiling of the iBMDM response to infection with either NC, Δ*thyA*, or Δ*hemB S. aureus* Newman was determined by TaqMan array analysis. Among the 90 immune genes tested, the transcription of 15 was uniquely elevated by Δ*thyA* relative to both NC and Δ*hemB* strains, including genes encoding chemokines (CXCL11, CXCL10, CCL5), pro-inflammatory interleukins (IL-6, IL-13, IL-12B, IL-1α, IL-1β), a transcription factor (STAT1), and cytokine/chemokine-induced regulators and receptors (SOCS1, CD40, CCR2, E-selectin) (**Figure 2A**). The mRNA levels of proinflammatory genes *Cxcl11*, *Il6*, *Cxcl10* and *Ccl5*, which were observed to be differentially induced by Δ*thyA* in the TaqMan arrays, were confirmed by qRT-PCR. In accordance with the TaqMan array data, these genes exhibited pronouncedly higher expression relative to NC and Δ*hemB* infected macrophages, with the control gene *Tnf* expressed comparably between all infecting strains (**Figure 2B**). These observations suggest that the Δ*thyA* strain stimulates higher expression of specific immune response genes during infection compared with other *S. aureus* strains.

Δ*thyA* activates STING through c-di-AMP

Cxcl11, *Cxcl10, Il6,* and *Ccl5*, which are expressed upon IRF3 or NF-κB activation through TBK1 (Abe and Barber, 2014; Balka et al., 2020; Chen et al., 2011, 2016), were differentially induced in Δ*thyA*-infected macrophages (**Figure 2B**). Since these inflammatory genes are co-regulated with *Ifnb*, which is downstream of IRF3 (Abe and Barber, 2014), *Ifnb1* mRNA and IFN-β protein levels in WT iBMDMs were measured by qRT-PCR and luciferase bioassay, respectively. As expected, Δ*thyA* induced higher IFN-β expression by iBMDMs compared to the NC and Δ*hemB* strains (**Figure 3A and B**).

IRF3-dependent induction of type I IFN in response to microbial pathogens can be triggered by activation of the cGAS-STING signaling pathway (Burdette et al., 2011; Ishikawa and Barber, 2008). Eukaryotic 2′3′-cGAMP, which is synthesized by cGAS in response to host or pathogen derived DNA, and bacterial cyclic dinucleotides can both activate STING, resulting in production of IFN-β (Burdette et al., 2011; Ishikawa and Barber, 2008; Zaver and Woodward, 2020) (**Figure 3C**). To reveal the mechanism(s) by which Δ*thyA* induces higher inflammation in macrophages, WT, *Sting*$^{-/-}$ and *cGas*$^{-/-}$ primary BMDMs (pBMDMs) were infected with either NC, Δ*thyA* or Δ*hemB S. aureus* Newman strains, and *Ifnb1* expression was measured by qRT-PCR. Δ*thyA* induced significantly higher *Ifnb1* transcription in all cell lines. Moreover, *Ifnb1* transcription was strikingly induced in WT but totally abolished in *Sting*$^{-/-}$ pBMDMs infected with Δ*thyA*, whereas *Ifnb1* expression was only slightly diminished in *cGas*$^{-/-}$ pBMDMs (**Figure 3D**). Consistent with the decreased *Ifnb1* expression in the *Sting*$^{-/-}$ pBMDMs, luciferase bioassays revealed that increased production of IFN-β protein in response to Δ*thyA* required the presence of STING but not cGAS (**Figure 3E**). These results indicated that *Ifnb1* induction by Δ*thyA* is primarily dependent on STING, rather than cGAS. We next measured the intracellular survival of NC, Δ*thyA* and Δ*hemB* strains in WT, *Sting*$^{-/-}$ and *cGas*$^{-/-}$ pBMDMs to determine if elevated activation of cGAS or STING contributes to *S. aureus* survival in tissue culture. In accordance with the observations in iBMDM and THP-1 cell lines, NC and Δ*hemB* exhibited similar survival trends, whereas Δ*thyA* exhibited significantly reduced persistence in all tested cell lines (**Figure S1**). Collectively, these findings indicate that the Δ*thyA* strain induces enhanced STING-dependent inflammation but STING signaling does not alter bacterial survival in tissue culture. Notably, induction of type I IFN production by the Δ*thyA* strain is STING dependent but largely cGAS/DNA independent.

Cyclic dinucleotides are key bacterial activators of STING. We therefore hypothesized that, relative to other *S. aureus,* TD-SCVs produce elevated levels of cyclic dinucleotides that more potently induce STING-dependent and cGAS-independent inflammation during infection. Bacteria are known to produce a diverse range of cyclic dinucleotides including c-di-GMP, c-di-AMP, 3′3′-cGAMP and others (Davies et al., 2012; Whiteley et al., 2019). However, *S. aureus* Newman is reported to lack functional enzymes to synthesize either 3′3′-cGAMP (Davies et al.,

2012) or c-di-GMP (Corrigan et al., 2011; Holland et al., 2008), and this strain also lacks alternative CD-NTase enzymes to synthesize other cyclic dinucleotides (Whiteley et al., 2019), suggesting that c-di-AMP is most likely the primary cyclic dinucleotide produced by this strain capable of activating STING. A Newman strain overexpressing the *S. aureus* di-adenylate cyclase DacA, which synthesizes c-di-AMP (Dengler et al., 2013), exhibited robust *Ifnb1* induction in iBMDMs (**Figure 3F**); in contrast, Δ*thyA* overexpressing the *Listeria monocytogenes* phosphodiesterase PdeA, which degrades c-di-AMP (Witte et al., 2013), eliminated *Ifnb1* induction (**Figure 3G**). C-di-AMP represents a key viability-associated pathogen-associated molecular pattern (vita-PAMPs) capable of activating STING to orchestrate host immune responses to live bacteria (Moretti et al., 2017). Heat-killing of bacterial cells abolishes c-di-AMP production and consequently blunts STING activation. To further verify that the *Ifnb1* induction by Δ*thyA* is due to c-di-AMP, we assessed the *Ifnb1* induction in iBMDMs by live or heat-killed NC, Δ*thyA* and Δ*hemB S. aureus* Newman strains (**Figure 3H**). As expected, unlike live *S. aureus*, heat-killed *S. aureus* did not induce *Ifnb1* expression. We also investigated the effects of c-di-AMP sequestration on *Ifnb1* induction by manipulating the expression of oxidoreductase RECON, which was identified previously by our laboratory as a high-affinity host receptor specific for bacterial cyclic dinucleotides (McFarland et al., 2017). RECON antagonizes STING activation by acting as a molecular sink for cyclic dinucleotides, including c-di-AMP, during bacterial infection in macrophages. To determine the effect of RECON overexpression on *Ifnb1* induction during Δ*thyA* infection, the WT, RECON overexpression (RECON OE) and knockdown (RECON KD) iBMDMs were each infected with NC and Δ*thyA S. aureus* Newman (**Figure 3I**). As expected, RECON overexpression disrupted the *Ifnb* induction by Δ*thyA*, whereas RECON knockdown significantly increased *Ifnb* expression. These results demonstrate that TD-SCVs activate STING signaling through c-di-AMP and induce STING-dependent inflammatory gene expression.

Δ*thyA* c-di-AMP levels are elevated under thymidine depletion

We next sought to investigate the effect of *thyA* deletion on production of c-di-AMP. Mutations in *thyA* disrupts dTMP (deoxythymidylate) synthesis from dUMP (deoxyuridylate), resulting in reliance on exogenous thymidine to maintain DNA synthesis (Zander et al., 2008). Supplementation of thymidine restored the growth defect of Δ*thyA* in BHI broth (**Figure 4A**). We then determined the effect of thymidine supplementation on c-di-AMP production. Relative to NC, intracellular c-di-AMP levels of Δ*thyA* were markedly increased upon thymidine starvation (1.25 μg/mL) compared with supplemental thymidine concentrations (2.5 and 5 μg/mL) that maximized growth (**Figure 4B**), indicating that thymidine availability regulates c-di-AMP production when *thyA* is inactivated. We then quantified the c-di-AMP levels in macrophages infected with NC, Δ*thyA* or Δ*hemB S. aureus* Newman strains. Consistent with our previous data, macrophages infected with Δ*thyA* had higher c-di-AMP levels relative to WT or Δ*hemB* infected cells (**Figure 4C**). We also determined c-di-AMP levels in macrophages infected with Δ*thyA* or the NC strain

grown in a range of thymidine concentrations, and in parallel we measured *Ifnb1* mRNA levels (**Figure 4D**). Macrophages infected with Δ*thyA* grown in lower concentrations of thymidine exhibited higher c-di-AMP levels and a correspondingly elevated *Ifnb1* transcriptional response, whereas both c-di-AMP and *Ifnb1* mRNA levels in macrophages infected with WT did not vary when grown in different thymidine concentrations (**Figure 4E and F**). These results support the hypothesis that Δ*thyA* inactivation in *S. aureus* leads to significantly higher c-di-AMP production in a thymidine-dependent manner, resulting in elevated type I IFN responses during macrophage infection.

S. aureus Δ*thyA* induces both STING-dependent and independent airway neutrophil inflammation

To compare the host responses to lung infection with different SCVs, WT mice were intranasally infected with either the Δ*thyA* or Δ*hemB* strain at an inoculum of 5×10^8 CFU. Lung bacterial burdens of SCVs differed significantly by 6 hpi in WT mice (**Figure 1F**). Therefore, we hypothesized that the host response to SCV infection would be apparent at early time points after infection. As neutrophils are the primary innate immune cell type in the defense against *S. aureus* infections (McGuinness et al., 2016), we measured the airway neutrophil burdens after infection. In WT mice, Δ*thyA* infection resulted in approximately 10-fold lower bacterial recovery from lung tissue (**Figure 5A**), but 10-fold higher airway neutrophil infiltration, relative to Δ*hemB* strains at 8 hpi (**Figure 5B**). The active neutrophil elastase concentration in bronchoalveolar lavage fluid (BALF), which reflects activated neutrophil levels, was also significantly higher in mice infected with Δ*thyA* than Δ*hemB* (**Figure 5C**). Moreover, Δ*thyA* was recovered with diminished abundance from lung tissue but induced higher neutrophil infiltration compared with the NC Newman strain (**Figure S2**). Surprisingly, *Ifnb1*, *Ifnl3* and *Isg15* expression was minimally induced compared to *Cxcl10* during infection with either Δ*thyA* and Δ*hemB* (**Figure 5D**), suggesting acute *S. aureus* infection does not strongly induce IFN production in the lung, and that other pathways downstream of STING are likely to be activated by Δ*thyA*. To further characterize the inflammatory response to this infection, we next performed a cytokine array assay of BALF collected during murine SCV infection. The cytokines CCL3 and G-CSF known to be responsible for neutrophil recruitment and mediating differentiation and maturation, respectively, were both elevated with Δ*thyA* infection (**Figure 5E**), with a 5-10-fold increase in BALF concentration compared with Δ*hemB* as confirmed by ELISA (**Figure 5F and G**).

To investigate if higher neutrophil infiltration and activation triggered by Δ*thyA* infection was controlled by STING, we then compared bacterial burdens and inflammatory responses of wild-type (WT) and *Sting*$^{-/-}$ mice infected with Δ*thyA*. Consistent with the tissue culture studies (**Figure S1**), *Sting* deletion did not affect bacterial survival at 8 hpi (**Figure 6A**). Furthermore, while *Sting*$^{-/-}$ mice demonstrated a nonsignificant trend towards decreased airway neutrophil infiltration compared with WT mice (**Figure 6B**), the neutrophil elastase concentration in BALF was

significantly decreased in *Sting*$^{-/-}$ mice (**Figure 6C**). Surprisingly, WT and *Sting*$^{-/-}$ mice exhibited comparable production of CCL3 (**Figure 6D**), indicating induction of CCL3 production by Δ*thyA* in the lung was largely STING independent. Consistent with the observed STING-dependent differences in active neutrophil elastase concentration, BALF levels of G-CSF, which is responsible for neutrophil activation, were significantly decreased in *Sting*$^{-/-}$ compared with WT mice (**Figure 6D**).

To confirm these observations, we then compared the effects in murine infections of NC Newman strain ectopically overexpressing the diadenylate cyclase DacA (NC/*dacA*) with the control strain (NC/vector) (**Figure 6E**). NC/*dacA* exhibited similar bacterial survival relative to control but induced significantly higher neutrophil infiltration and activation as assessed by active elastase concentration in WT mice at 8 hpi (**Figure 6F and G**). Similarly, NC/*dacA* yielded comparable levels of CCL3 and significantly higher G-CSF production relative to NC/vector, confirming that elevated CCL3 induction by Δ*thyA in vivo* is independent of both STING and c-di-AMP, but that G-CSF is promoted through this signaling axis. Previous reports have shown that CCL3 can be directly induced by administration of purified cyclic dinucleotides (Mahmoud et al., 2020). We also observed that intranasal instillation of c-di-AMP resulted in higher CCL3 in BALF of WT mice, but not in *Sting*$^{Gt/Gt}$ mice (**Figure S3**), however the levels of cytokine were much lower than those observed during SCV infection. Taken together, these results indicate that during Δ*thyA* infection, the majority of CCL3 induction was STING-independent and attributable to another, as-yet undefined characteristic unique to the TD-SCV subtype. Additionally, the augmented immune response includes increased production of G-CSF through STING activation, boosting the maturation and activation of neutrophils.

Hypertonic saline and CCL3 signal blockade control lung inflammation caused by TD-SCV infection

While antibiotic therapy is commonly used to treat CF lung infections, the emergence of antibiotic resistance, exemplified by TD-SCVs, limits the efficacy of these treatments. Previous studies, and our observations above, suggested alternative targets for addressing the adverse clinical effects of TD-SCV infections. For example, we previously observed the prevalence of TD-SCVs to be lower among children treated with hypertonic saline (Wolter et al., 2019), a common CF mucolytic therapy (Donaldson et al., 2006; Reeves et al., 2012). C-di-AMP is a critical regulator of bacterial osmolyte transport, and of resulting cell integrity (Gibhardt et al., 2019; Huynh et al., 2016; Moscoso et al., 2016; Schuster et al., 2016). Consequently, high osmolarity conditions inhibit the growth of bacteria with high c-di-AMP production (Turner et al., 2020). Based on these observations, we hypothesized that the lower TD-SCV prevalence we observed among children treated with hypertonic saline was attributable to increased c-di-AMP levels. We therefore defined the effects of increasing concentrations of NaCl on the growth of NC and Δ*thyA S. aureus* strains, and the effects of thymidine supplementation. Under conditions of thymidine repletion (2.5 or 5

μg/mL thymidine), we observed no effects of varying NaCl concentrations on growth of NC and Δ*thyA*. However, with 1.25 μg/mL of thymidine, in which Δ*thyA* produces elevated c-di-AMP, Δ*thyA in vitro* growth yields decreased 2 logs in 5% NaCl, an effect not observed for NC *S. aureus* regardless of thymidine concentration (**Figure 7A and B**), suggesting c-di-AMP mediates the susceptibility of Δ*thyA* to osmotic stress.

Neutrophil inflammation and airway damage are central to the pathogenesis of CF lung disease. CCL3 recruits monocytes or granulocytes to the site of inflammation by binding to its receptor, CCR1 and functions as a key mediator of lung injury in mouse pulmonary disease models (Ishida et al., 2007; Yang et al., 2011). Treatment with CCR1 antagonist BX-471 has been shown to diminish neutrophil recruitment to the lung (Yang et al., 2011). Given that Δ*thyA* induced approximately 5-fold higher CCL3 production than Δ*hemB* during murine lung infections (**Figure 5F**), we hypothesized that pharmacological blockade of this signaling axis may prevent neutrophil enervation into the airway. Accordingly, we tested whether BX-471, a CCR1 inhbitor, blocks induction of neutrophil infiltration and impacts infection dynamics by Δ*thyA* in WT mice. Administration of BX-471 to mice 30 min before infection resulted in elevated lung tissue bacterial burdens at 8 hpi (**Figure 7C**). Nevertheless, and despite the increased bacterial densities, this brief treatment was sufficient to block neutrophil infiltration (**Figure 7D**). Taken together, these results suggest that CCL3 signal blockade combined with hypertonic saline administration could effectively prevent neutrophil recruitment into the airway and facilitate clearance of TD-SCVs, respectively, ultimately reducing tissue damage.

DISCUSSION

Antibiotics are commonly administered to treat CF lung infections. However, antibiotic treatment has been linked to the emergence of antibiotic-resistant SCVs, which can establish persistent infections and are associated with markedly worse lung disease severity (Kriegeskorte et al., 2015; Suwantarat et al., 2018). In the current study, we found that *S. aureus* TD-SCVs are also hyperinflammatory during infection of both phagocytes *ex vivo* and the murine lung *in vivo*, promoting airway neutrophil infiltration. This elevated host response depended at least in part upon increased c-di-AMP levels in *S. aureus* and STING activation in host cells. Elevated c-di-AMP levels were inversely associated with exogenous thymidine concentrations, which are known to vary in human airway secretions (Zander et al., 2010). How c-di-AMP levels are linked to thymidine metabolism and utilization remains unclear, but c-di-AMP biosynthesis may be directly affected by thymidine utilization, or indirectly moderated by thymidine starvation. C-di-AMP levels have been linked to metabolic regulation in several bacteria; conversely, metabolic changes are also known to alter c-di-AMP levels (Sureka et al., 2014). The DNA synthesis precursor dTMP can be synthesized either from dUMP by ThyA, or from thymidine by thymidine kinase (TMK), respectively (Zander et al., 2008). Consequently, disruption of *thyA* causes *S. aureus* to rely on

exogenous thymidine for growth, which is imported by the NupC nucleoside transport system, followed by phosphorylation by TMK. Interestingly, in *S. aureus,* the gene *tmk* is in a conserved operon with the gene encoding a c-di-AMP receptor, PII-like signal transduction protein A (*pstA*) (Choi et al., 2015; Müller et al., 2015). While it is conceivable that c-di-AMP directly regulates thymidine uptake and metabolism, other observations suggest a different relationship may link these processes. For example, thymidine depletion is known to induce DNA damage (Besier et al., 2009), and c-di-AMP signaling has been implicated in the repair of DNA lesions (Oppenheimer-Shaanan et al., 2011). It is therefore tempting to speculate that c-di-AMP levels in TD-SCVs are modulated by pyrimidine metabolism and/or DNA repair, all of which are impacted by thymidine starvation.

Alternatively, c-di-AMP levels in TD-SCVs may be increased indirectly due to other altered cellular functions. For example, cells of Δ*thyA* mutants have been shown to be markedly enlarged during thymidine limitation, exhibiting approximately three times the volume of WT cells (Kriegeskorte et al., 2014). C-di-AMP levels may be modulated in response to distorted cellular structure, perhaps supporting cell integrity. Bacteria import ions and osmolytes to maintain cellular turgor in response to fluctuating environmental osmotic pressure. C-di-AMP is a general osmotic stress regulator involved in regulating uptake of potassium and compatible solutes. Modulation of c-di-AMP by *S. aureus* is also known to regulate cell size and to moderate the effects of extreme membrane and cell wall stress by reducing cell size and altering the composition of cell wall (Corrigan et al., 2011; Zeden et al., 2018). Therefore, increased c-di-AMP production may help compensate for the enlarged cell size characterized by *thyA* mutation. Consistent with a role in osmotic stress response and cellular stability, we found that TD-SCVs were sensitive to high salt. Hypertonic saline inhibited the growth of TD-SCVs, especially in low thymidine concentrations, which further increase c-di-AMP levels. Clinical observations are further supportive of this concept: Wolter and colleagues found the prevalence of TD-SCVs to be significantly lower among CF patients receiving hypertonic saline (Wolter et al., 2019). Therefore, hypertonic saline treatment may facilitate the clearance of TD-SCVs through a c-di-AMP-dependent mechanism.

Our study coupled STING and CCL3-dependent inflammation with neutrophil infiltration and activation in response to TD-SCV infection in the airway. Neutrophils protect the host against bacterial infection by production of neutrophil extracellular traps (NETs), non-specific antimicrobial molecules and anti-microbial proteases and peptides (Porto and Stein, 2016). However, persistent neutrophil recruitment and activation can lead to overexuberant, and maladaptive, tissue damage (McGuinness et al., 2016). Therefore, the relatively high neutrophil recruitment elicited by TD-SCV infection is predicted to worsen airway wall damage and lung function decline; our results suggest blockade of CCL3 may prevent these effects.

Our results also underscore the likely importance of STING in CF lung disease. CF patients have chronic polymicrobial airway infections, resulting in a complex milieu of proinflammatory

ligands that includes DNA from dead neutrophils, c-di-AMP from organisms like *S. aureus*, and c-di-GMP from *P. aeruginosa*, another key CF respiratory pathogen. Such an environment may result in chronic STING activation, reminiscent of the autoimmune disease **S**TING-**A**ssociated **V**asculopathy with onset in **I**nfancy (SAVI). SAVI results from gain-of-function mutations and constitutive STING activation (Liu et al., 2014), and is characterized by systemic vasculopathy and lung disease. While vascular pathology is entirely dependent upon STING induction of type I IFN, lung disease and fibrosis are independent of IRF3 or type I IFN (Luksch et al., 2019; Motwani et al., 2019; Warner et al., 2017). These observations together with reports that administration of cyclic dinucleotides to the lung failed to induce mucosal type I IFN production (Blaauboer et al., 2014, 2015; Van Dis et al., 2018) collectively suggest that alternative STING signaling mechanisms exist in the lung and that chronic activation of STING in this context can contribute to disease pathology and lung fibrosis. Besides gain-of-function mutations, a significant proportion of humans have STING alleles competent for cGAS signaling but that are unresponsive to bacterial derived cyclic dinucleotides (Yi et al., 2013), suggesting that some CF patients may be resistant to the pathology associated with chronic STING activation. Future studies detailing the impacts of STING and CCL3 activation in the context of CF and other chronic infections associated with TD-SCVs may provide new therapeutic interventions to prevent pathology associated with their unexpected hyperinflammatory properties.

In summary, our study revealed a previously neglected aspect of STING signaling in the lung by characterizing the inflammatory capacity of c-di-AMP producing SCVs, and provided a potential mechanistic explanation for TD-SCV associated lung function decline among people with CF. Furthermore, our study demonstrated potential therapeutic methods to control TD-SCV infection and detrimental neutrophil activity, which may provide insight for the treatment against the infection of different SCV subtypes in people with CF and other chronic bacterial infections.

ACKNOWLEDGMENTS

We would like to thank Daniel B. Stetson for providing *Tmem173*$^{-/-}$ and *cGAS*$^{-/-}$ mice. We thank Jessica M. Snyder at Department of Comparative Medicine, University of Washington for the help with handling mouse tissue samples. Q.T. was supported by the University of Washington Cystic Fibrosis Foundation RDP Fellowship (SINGH15R0). This work was supported by a Pilot and Feasibility Award from the Cystic Fibrosis Foundation (WOODWA16I0) and NIH Grant R01 AI139071.

AUTHOR CONTRIBUTIONS

Q.T. and J.J.W. conceived and designed the research. Q.T., M.R.P., M.T., and F.A.Q. performed experiments. Q.T., M.T., A.P.M. and J.J.W. provided key insights. D.W. and L.R.H provided key

tools and reagents. Q.T. and J.J.W. analyzed the data and wrote the paper. All authors reviewed the manuscript prior to submission.

DECLARATION OF INTERESTS

The authors declare no competing interests.

MAIN FIGURE TITLES AND LEGENDS

Figure 1. Δ*thyA* exhibits decreased survival during macrophages or murine lung infection. (A) Auxotrophy test for thymidine and hemin dependence in the deletion strains. Representative image of a lawn of Δ*thyA* or Δ*hemB* plated on Mueller-Hinton agar and showing enhanced growth around the paper disk impregnated with thymidine or hemin, respectively. The arrows indicate bacterial growth around the disk. (B) Bacterial survival curves of NC, Δ*thyA*, and Δ*hemB S. aureus* Newman strains in iBMDM cells. Mean values of duplicates are plotted and error bars indicate ±SD. *P* values were calculated using Two-way ANOVA analysis. (C) LDH release of iBMDMs infected with indicated *S. aureus* Newman strains at 4 hpi normalized to 100% lysis controls. Mean values of duplicates are plotted and error bars indicate ±SD. *P* values were calculated using One-way ANOVA analysis. (D) Bacterial survival curves of NC, Δ*thyA*, and Δ*hemB S. aureus* Newman strains in THP-1 cells. THP-1 cells were differentiated by 100 nM PMA for 3 days before infection. Mean values of duplicates are plotted and error bars indicate ±SD. *P* values were calculated using Two-way ANOVA analysis. (E) LDH release of THP-1 cells differentiated as in panel (D) infected with indicated *S. aureus* Newman strains at 4 hpi normalized to 100% lysis controls. Mean values of duplicates are plotted and error bars indicate ±SD. *P* values were calculated using One-way ANOVA analysis. (F) Bacterial recovery from the lung of WT C57BL/6J mice intranasally infected with Δ*thyA* and Δ*hemB*. Horizontal black bars are the median of the measured bacterial burdens. *P* values were calculated using Mann-Whitney analysis. For all panels, Asterisks indicate that differences are statistically significant (*, $P < 0.05$; **, $P < 0.01$; ***, $P < 0.001$), and ns indicates no significant difference.

Figure 2. Δ*thyA* promotes elevated inflammation during macrophage infection. (A) Heatmap of Taqman gene expression analysis of WT iBMDMs infected with NC, Δ*thyA*, and Δ*hemB S. aureus* Newman strains. Values are the $\log_2$ ratio of differences in the transcription of the indicated genes (Δ*thyA* vs NC and Δ*thyA* vs Δ*hemB*). Heatmaps were generated using Morpheus (https://software.broadinstitute.org/morpheus). (B) Transcriptional differences for genes labeled green in panel (A) were confirmed by qRT-PCR in iBMDMs. Un indicates uninfected controls. Mean values of duplicates are plotted and error bars indicate ±SD. For all panels, *P* values were calculated using One-way ANOVA analysis. Asterisks indicate that differences are statistically significant (*, $P < 0.05$; **, $P < 0.01$; ***, $P < 0.001$, ****, $P < 0.0001$), and ns indicates no significant difference.

Figure 3. Δ*thyA* activates STING dependent type I IFN production through c-di-AMP in macrophages. (A) WT iBMDMs were infected with NC, Δ*thyA* and Δ*hemB* Newman strains for 4 hrs, and *Ifnb1* mRNA was measured by qRT-PCR relative to uninfected controls. Mean values of duplicates are plotted and error bars indicate ±SD. (B) Infections performed as in (A) for 6 hrs, and IFN-b protein was measured by ISRE-luciferase bioassay. Mean values of 6 replicates are plotted and error bars indicate ±SD. (C) Schematic diagram of STING activation. Eukaryotic 2′3′-cGAMP, synthesized by cGAS that is triggered by host or pathogen derived DNA, and bacterial cyclic dinucleotides can both active STING, resulting in IFN-β induction. (D) WT, *Sting* $^{-/-}$ and *cGas*$^{-/-}$ pBMDMs were infected with NC, Δ*thyA* and Δ*hemB* Newman strains for 4 hrs, and induction of *Ifnb1* transcripts were measured by qRT-PCR relative to uninfected controls incubated for the same time. Mean values of triplicates are plotted and error bars indicate ±SD. (E) Infections performed as in (D) for 6 hrs, and IFN-β protein was measured by ISRE-luciferase bioassay. Mean values of triplicates are plotted and error bars indicate ±SD. (F) *Ifnb1* expression in iBMDMs infected with NC, *dacA* overexpression, or Δ*thyA* Newman strains relative to uninfected control. Mean values of duplicates are plotted and error bars indicate ±SD. (G) The *Ifnb1* expression in iBMDMs infected with NC, Δ*thyA*, and *Listeria monocytogenes pde* (*Lmpde*) overexpression Newman strains relative to uninfected control. Mean values of duplicates are plotted and error bars indicate ±SD. (H) *Ifnb1* induction in iBMDMs by live or heat-killed NC, Δ*thyA* and Δ*hemB* Newman strains with the same starting CFU assayed at 4 hpi. Mean values of duplicates are plotted and error bars indicate ±SD. (I) *Ifnb1* expression in WT, RECON overexpression (RECON OE) or knockdown (RECON KD) iBMDMs infected with NC or Δ*thyA* Newman strains relative to uninfected controls. Mean values of duplicates are plotted and error bars indicate ±SD. For all panels, *P* values were calculated using One-way or Two-way ANOVA analysis. Asterisks indicate that differences are statistically significant (*, $P < 0.05$; **, $P < 0.01$; ***, $P < 0.001$, ****, $P < 0.0001$), and ns indicates no significant difference.

Figure 4. Thymidine affects c-di-AMP levels and STING activating capacity of TD-SCV. (A) Growth curve of NC (left panel) and Δ*thyA* (right panel) *S. aureus* Newman in BHI broth supplemented with the indicated concentration of thymidine. Mean values of duplicates are plotted and error bars indicate ±SD. (B) LC-MS/MS detection of c-di-AMP levels of NC and Δ*thyA* grown in BHI broth supplemented with the indicated concentrations of thymidine. Mean values of duplicates are plotted and error bars indicate ±SD. (C) LC-MS/MS quantification of intracellular c-di-AMP in iBMDMs infected with NC, Δ*thyA* and Δ*hemB* Newman strains for 4 hrs. Mean values of duplicates are plotted and error bars indicate ±SD. (D) Schematic diagram of macrophage infection, in which WT iBMDMs were infected with NC or Δ*thyA* overnight culture grown in BHI broth supplemented with the indicated thymidine concentrations for 4 hrs, the intracellular c-di-AMP levels and *Ifnb1* expression in iBMDMs were determined by LC-MS/MS and qRT-PCR, respectively. Mean values of duplicates are plotted and error bars indicate ±SD. (E) The

intracellular c-di-AMP concentration in iBMDMs as in panel (D). Mean values of duplicates are plotted and error bars indicate ±SD. (F) Infections performed as in (D) and *Ifnb1* mRNA was measured by qRT-PCR relative to uninfected control. Mean values of duplicates are plotted and error bars indicate ±SD. For all panels, *P* values were calculated using One or Two-way ANOVA analysis. Asterisks indicate that differences are statistically significant (**, $P < 0.01$; ****, $P < 0.0001$).

Figure 5. TD-SCV induces robust airway neutrophil infiltration. (A) WT mice were intranasally infected with either Δ*thyA* or Δ*hemB* strains. The CFU recovery from the right lung were numerated at 8 hpi. (B) The neutrophils in BAFL of the mice infected as in panel (A) were identified and enumerated by FACS assay. (C) Active neutrophil elastase concentration in BALF form mice infected as in panel (A). (D) *Ifnb1*, *Ifnl3*, *Isg15* and *Cxcl10* expression in the lungs measured by qRT-PCR. (E) Heatmap of BALF cytokine array analysis of WT mice infected with Δ*thyA* or Δ*hemB* for 8 hrs. Values are the $\log_2$ ratio of differences in the concentration of the indicated cytokines (Δ*thyA* vs Δ*hemB*). Cytokines responsible for neutrophil recruitment and activation were highlighted in green. (E) BALF CCL3 and G-CSF concentration of mice infected as panel (A) determined by ELISA. For all panels, horizontal black bars indicate the median of the data. *P* values were calculated using Mann-Whitney analysis. Asterisks indicate that differences are statistically significant (*, $P < 0.05$; **, $P < 0.01$; ***, $P < 0.001$, ****, $P < 0.0001$), and ns indicates no significant difference.

Figure 6. STING controls the airway neutrophil activation induced by TD-SCV infection. (A) WT or *Sting*$^{-/-}$ mice were intranasally infected with Δ*thyA*. The CFU recovery from the right lung were numerated at 8 hpi. (B) The neutrophils present in BAFL collected from the mice infected as in panel (A) were identified and numerated by FACS assay. (C) Active neutrophil elastase concentration in BALF. (D) BALF CCL3 and G-CSF concentration of mice infected as panel (A) determined by ELISA. (E) Wild mice were intranasally infected with DacA overexpression (NC/dacA) or its control (NC/vector) Newman strain. The CFU recovery from the right lung were enumerated at 8 hpi. (F) The neutrophils present in BAFL collected from the mice infected as in panel (E) were identified and numerated by FACS assay. (G) Active neutrophil elastase concentration in BALF. (H) BALF CCL3 and G-CSF concentration of mice infected as panel (E) determined by ELISA. For all panels, horizontal black bars are the median of the data. *P* values were calculated using Mann-Whitney analysis. Asterisks indicate that differences are statistically significant (*, $P < 0.05$; **, $P < 0.01$; ***, $P < 0.001$, ****, $P < 0.0001$), and ns indicates no significant difference.

Figure 7. Controlling lung inflammation caused by TD-SCV colonization. (A) The growth of NC and Δ*thyA* on BHI agar plates supplemented with indicated concentration of thymidine in presence or absence of 5% of NaCl. Mean values of duplicates are plotted and error bars indicate

±SD. (B) The OD_{600} of NC and Δ*thyA* grown in BHI broth supplemented with 5% of NaCl relative to bacteria grown in normal BHI medium. Mean values of duplicates are plotted and error bars indicate ±SD. *P* values were calculated using Two-way ANOVA analysis. (C) WT mice were subcutaneously injected with BX-471 (100 mg/kg) or DMSO 30 minutes before intranasal Δ*thyA* infection. Bacterial recovery of the right lung was numerated at 8 hpi. Horizontal black bars are the median of the data. *P* values were calculated using Mann-Whitney analysis. (D) The neutrophil count in BALF collected from mice infected as in panel (C) was identified and numerated by FACS assay. Horizontal black bars indicate the median of the data. For all panels, *P* values were calculated using Mann-Whitney analysis. Asterisks indicate that differences are statistically significant (*, $P < 0.05$; **, $P < 0.01$; ***, $P < 0.001$, ****, $P < 0.0001$), and ns indicates no significant difference.

STAR METHODS

RESOURCE AVAILABILITY

Lead Contact

Please direct any requests for further information or reagents to the lead contact, Joshua J. Woodward (jjwoodwa@uw.edu).

Materials Availability

This study did not generate new unique reagents. Reagents are as described in Key Resources Table.

Data and Code Availability

This study did not generate or analyze new datasets or codes.

EXPERIMENTAL MODEL AND SUBJECT DETAILS

Microbe Strains and Culturing Conditions

S. aureus Newman was grown in brain heart infusion (BHI) broth and incubated at 37 °C with shaking. *Escherichia coli* used for cloning was grown in Lysogeny broth (LB) at 37 °C with shaking. Hemin-dependent and thymidine-dependent SCVs were grown in BHI broth supplemented with thymidine or hemin at the indicated concentration. When necessary, relevant antibiotics were added to the cultures with the following final concentration: 1 μg/ml anhydrotetracycline and 10 μg/ml chloramphenicol.

Human Cell Line

Human THP-1 cells (ATCC) were cultured in RPMI medium supplemented with 10% heat-inactivated FBS and 1% penicillin/streptomycin. THP-1 cells were differentiated by 100 nM PMA for 3 days before *S. aureus* infection.

Murine Cell Lines

Bone marrow from WT, *cGas*$^{-/-}$, and *Tmem173*$^{-/-}$ mice were generously provided by Daniel Stetson at the University of Washington. Primary BMDMs were generated as previously described (Weischenfeldt and Porse, 2008). J2 virus immortalized BMDM cell line was from Dan Portnoy at the University of California, Berkeley. Both the primary and immortalized BMDMs were cultured in Dulbecco's Modified Eagle Medium (DMEM) supplemented with 2 mM sodium glutamine, 1 mM sodium pyruvate, 10% heat-inactivated FBS, 0.1% 2-Mercaptoethanal, 10% L929 cell supernatants as a source of M-CSF and 1% penicillin/streptomycin.

Mice

All the mice used in this study were on C57BL/6J background. The original breeding pairs of WT and *Sting*$^{Gt/Gt}$ were from Jackson Laboratories, *Tmem173*$^{-/-}$ were donated by Daniel Stetson at the University of Washington (Brunette et al., 2012). Mice colonies were bred and maintained under SPF conditions and ensured through the rodent health monitoring program overseen by the Department of Comparative Medicine at the University of Washington. All experiments involving mice were performed in compliance with guidelines set by the American Association for Laboratory Animal Science (AALAS) and were approved by the Institutional Animal Care and Use Committee (IACUC) at the University of Washington. All experiments were carried out with mice aged 8-12 weeks matched by gender, age and body weight.

METHOD DETAILS

Laboratory *S. aureus* SCVs construction

S. aureus Newman Δ*thyA* and Δ*hemB* strains were constructed by allelic exchange using pIMAY (Monk et al., 2012). Briefly, primers were designed to amplify upstream and downstream regions flanking the gene(s) of interest (either *thyA* or *hemB*) to delete the entire open reading frame (**Table S1**). Genomic DNA from *S. aureus* strain Newman was used as a template to generate fragments consisting of linked sequences upstream and downstream of either *thyA* or *hemB* (Δ*thyA* or Δ*hemB* cassette) by overlapping PCR. The amplimer was cloned into pIMAY and transformed via electroporation into *E. coli* DH10B and then transformed into *S. aureus* strain RN4220. Transduction of *S. aureus* strain Newman was accomplished by first propagating phage ϕ-11 (to package the pIMAY vector) in RN4220 that had been successfully transformed with pIMAY_deletion cassette (Δ*thyA* or Δ*hemB*). Allelic exchange of either Δ*thyA* or Δ*hemB* was achieved by subsequent generalized phage transduction of the appropriate ϕ-11 pIMAY_deletion cassette vector into strain Newman. The resulting SCV strains were confirmed by PCR and further tested for auxotrophy for either thymidine or hemin; both showed attenuated growth in vitro compared with the wild-type Newman strain in the absence of either thymidine or hemin.

Macrophage infection with *S. aureus*

For *S. aureus* infection of macrophages, 1×10^6 cells were plated in 6-well tissue culture plates and incubated at 37 °C in 5% carbon dioxide (CO_2) overnight. Mid-exponential phase *S. aureus* cultures were washed twice with sterile phosphate-buffered saline (PBS) and then re-suspended in DMEM medium. The macrophages were infected by *S. aureus* at a multiplicity of infection of 100. After a 1 hr incubation, the cells were washed twice with PBS and given fresh DMEM medium containing 100 μg/ml gentamicin to kill the extracellular bacteria. At various times post-infection, supernatants were collected to study macrophage cell death by lactate dehydrogenase (LDH) release assays (Promega, USA) (Smith et al., 2011), IFN-β protein expression by luciferase bioassays (Woodward et al., 2010), and cells were collected for RNA isolation. For the luciferase bioassay, supernatants were applied in various dilutions to the IFN responsive ISRE-L929 cells (5×10^4 cells/well, 96-well plate). Cells were incubated for 6 hrs, the media was aspirated, and 50 μL of TNT lysis buffer (20 mM Tris, 100 mM NaCl, 1% Triton X-100) was added to each well. 40 μL of the lysate was mixed with 40 μL of luciferase substrate solution (20 mM Tricine, 2.67 mM $MgSO_47H_2O$, 0.1 mM EDTA, 33.3 mM DTT, 530 μM ATP, 270 μM acetyl CoA lithium salt, 470 μM luciferin, 5 mM NaOH, 265 μM magnesium carbonate hydroxide and luminescence was measured using a Synergy HT (BioTek, USA). For intracellular CFU enumeration, macrophages were lysed in PBS containing 0.1% Triton X-100 and incubated at 37 °C for 5 min. Appropriate dilutions were plated on BHI agar plates and incubated at 37 °C overnight and CFU were enumerated.

***In vivo S. aureus* infection and bacterial burden estimation**

Mice aged 8-12 weeks were used in infection experiments. Prior to animal experiments, overnight cultures of NC, Δ*thyA* and Δ*hemB* were back diluted twice (OD_{600}=0.15) and grown for 2 h at 37 °C with 5 μg/mL of thymidine and 1 μg/mL hemin in BHI broth, respectively, to reach mid-exponential growth. Subsequently, the bacteria were washed once with PBS. Cultures were diluted in PBS to achieve a final inoculum of 5×10^8 bacteria and used to infect mice via the intranasal route while the animals were anesthetized with isoflurane. For the BX-471 administration, mice were subcutaneously injected with BX-471 (100 mg/kg) or DMSO alone 30 minutes before intranasal Δ*thyA* infection. Mice were euthanized and lungs collected at the indicated time points. Lungs were homogenized and lysed in 5 mL PBS using a Tissue Tearor Homogenizer. Bacterial burdens were enumerated by plating dilutions on BHI plates containing thymidine or hemin to ensure the normal growth of SCVs.

TaqMan array experiments and relative quantitative real-time PCR

The left lungs of mice were sliced into pieces no wider than 0.5 cm and dropped into RNAlater (Thermo Fisher Scientific, USA) for RNA stabilization. At the time of RNA isolation, the samples were removed from RNAlater and homogenized by Bead Mill homogenizer (Thermo Fisher Scientific, USA) in Lysis buffer from NucleoSpin RNA Plus Kit (Clontech, USA). RNA from the

lung homogenate or macrophages was isolated using NucleoSpin RNA Plus Kit (Clontech, USA) followed by cDNA synthesis using iScript cDNA synthesis Kits (Bio-Rad, USA) following manufacturer's instructions. QRT-PCR was performed using TaqMan Gene expression master mix (Thermo Fisher Scientific, USA). Taqman probes for mouse genes were pre-designed assays from Thermo Fisher Scientific. To calculate mRNA fold change, transcript levels were determined by normalizing to mouse *Hprt* using the $2^{(-\Delta\Delta Ct)}$ method. Immune gene expression profiling was performed using TaqMan Array Micro Fluidic Cards (Applied Biosystems, USA) containing probe sets for 90 immune genes and 6 endogenous controls.

Flowcytometry analysis for BAL neutrophils

Mice were sacrificed at the indicated time by CO_2 asphyxiation and lungs were lavaged with 0.5 ml ice-cold PBS twice. A total of 1 mL of lavage fluid was centrifuged at 2,000 g for 2 min. Collected cells were re-suspended in 100 µL Red Cell Lysis Buffer (BioLegend, USA) and incubated for 5 min. Cells lysis was stopped by adding 400 µL Cell Staining Buffer (BioLegend, USA). Cells were then centrifuge for 2 min at 2,000 g for 2 min and re-suspend in Cell Staining Buffer. Viable cells were counted using the Automatic cell counter (Bio-Rad) after trypan blue staining. Fc receptors were blocked by incubating cells with TruStain FcX™ PLUS anti-mouse CD16/32 antibody (Biolegend, USA) for 10 min. Dead cells were stained using the Zombie Green Fixable Viability Kit (BioLegend, USA) for 10 min. Cells were wash twice with 500 µL PBS and resuspend in Cell Staining Buffer. Cells were thereafter stained with antibodies for the desired surface markers for 20 min on ice in the dark. Flow cytometric data were acquired on Cytek Aurora analyzed using the FlowJo software. The following antibodies specific for the cell surface antigens from Biolegend were used in the flow cytometry: Brilliant Violet 421 anti-mouse Ly-6G, PE/Dazzle 594 anti-mouse/human CD11b, PerCP/Cyanine5.5 anti-mouse CD45, PE anti-mouse F4/80. 10, 000 live singlet cells were pre-gated. Neutrophils were identified as live, $CD45^+$, $F4/80^-$, $CD11b^+$, $Ly6G^+$ (**Figure S4**). The neutrophil numbers were calculated according to total cells in BALF and the percent of neutrophil identified by FACS assay.

Intranasal c-di-AMP administration

C57BL/6J WT and *Sting*$^{Gt/Gt}$ mice aged of 8-12 weeks were anesthetized under isoflurane. Mice were intranasally instilled with either sterile 15 mg c-di-AMP in PBS or sterile PBS alone and sacrificed at 8 hrs after treatment. The BALF CCL3 concentration was measured at 8 hpi by Mouse CCL3/MIP-1 alpha Quantikine ELISA Kit (R&D, USA).

Neutrophil elastase assay

Elastase activity was measure by spectrofluorometrically monitoring the hydrolysis product of the fluorogenic substrate MeOSuc-AAPV-AMC (Cayman, USA). BALF was centrifuged at the maximum speed to remove the cell debris. 20 µL BALF was mixed with 80 µL substrate solution (0.1 mM MeOSuc-AAPV-AMC, 0.5 M NaCl, 0.01 M $CaCl_2$, 10% DMSO, 0.05 M Tris, pH 7.5)

in white bottom plates. The kinetics of substrate cleavage (increase in fluorescence of the liberated 7-amino-4-methylcoumarin, AMC) was measured using a fluorometer (BioTek, USA) set at 370 nm excitation and 460 nm emission at 37°C. Porcine elastase (Sigma, USA) was used to generate a standard curve.

Mouse cytokine array and ELISA assay

The relative levels of mouse cytokines in BALF were determined by using the Mouse XL Cytokine Array Kit (R&D, USA) according to the manufacturer's instructions. The chemiluminescence of the membranes were collected and analyzed by an Odyssey Fc imaging system (Li-Cor BioSciences, USA). CCL3 and G-CSF concentrations in the BALF were measured by using the Mouse Quantikine ELISA Kit (R&D, USA).

Quantification of c-di-AMP by LC-MS/MS

Overnight culture of NC, Δ*thyA* and Δ*hemB* strains grown in BHI supplemented with 5 μg/mL of thymidine were washed twice by PBS, then diluted into fresh BHI containing various concentration of thymidine (1.25, 2.5 and 5 μg/mL) with the initial OD_{600} of 0.05, and grown at 37 °C with shaking for 4 hrs. The bacteria were collected by centrifugation (2,700 × g, 5 min) and used for c-di-AMP extraction or macrophage infection. Macrophages infected with bacteria were collected by incubating in 0.05% Trypsin-EDTA for 5 min. Both macrophages and bacteria were re-suspended in methanol and lysed by sonication. Heavy-labeled (^{3}H) c-di-AMP was added into the extract as the internal control. Bacterial lysates were centrifuged to collect cell-free supernatants. The quantification of c-di-AMP by LC-MS was performed as previously described (Huynh et al., 2015).

QUANTIFICATION AND STATISTICAL ANALYSIS

All numerical data were analyzed and plotted using GraphPad Prism 6.0 software. Statistical parameters are reported in the Figure Legends.

SUPPLEMENTAL FIGURE TITLES AND LEGENDS

Table S1. Oligonucleotides used in this study.

Figure S1. Bacterial survival in WT, *Sting* $^{-/-}$ and *cGas* $^{-/-}$ pBMDMs. Mean values of duplicates are plotted and error bars indicate ±SD. *P* values were calculated using Two-way ANOVA analysis. Asterisks indicate that differences are statistically significant (*, $P < 0.05$; **, $P < 0.01$; ***, $P < 0.001$, ****, $P < 0.0001$).

Figure S2. Δ*thyA* induces higher airway neutrophil infiltration than NC strain. (A) WT mice were intranasally infected with the Δ*thyA* or NC strains. The CFU recovery from the right lung were enumerated at 8 hpi. (B) The neutrophils in BAFL of the mice infected as in panel (A) were

identified and enumerated by FACS assay. For all panels, the horizontal black bar is the median of the data. *P* values were calculated using Mann-Whitney analysis. Asterisks indicate that differences are statistically significant (**, $P < 0.01$).

Figure S3. C-di-AMP induces CCL3 production in STING dependent manner. WT or *Sting*$^{Gt/Gt}$ mice were intranasally instilled with 15 mg c-di-AMP in PBS or PBS control (CTRL). The BALF CCL3 concentration was measured at 8 hpi by ELISA. The horizontal black bar is the median of the data. *P* values were calculated using Mann-Whitney analysis. Asterisks indicate that differences are statistically significant **, $P < 0.01$), and ns indicates no significant difference.

Figure S4. Gating strategy. Neutrophils were identified as live, CD45$^+$, F4/80$^-$, CD11b$^+$, Ly6G$^+$.

REFERENCES

Abe, T., and Barber, G.N. (2014). Cytosolic-DNA-mediated, STING-dependent proinflammatory gene Induction necessitates canonical NF-κB activation through TBK1. J. Virol. *88*, 5328-41. doi: 10.1128/JVI.00037-14.

Alonzo, F., and Torres, V.J. (2014). The bicomponent pore-forming leucocidins of *Staphylococcus aureus*. Microbiol. Mol. Biol. Rev. *78*, 199-230.

Balka, K.R., Louis, C., Saunders, T.L., Smith, A.M., Calleja, D.J., D'Silva, D.B., Moghaddas, F., Tailler, M., Lawlor, K.E., Zhan, Y., et al. (2020). TBK1 and IKKε act redundantly to mediate STING-induced NF-κB responses in myeloid cells. Cell Rep. *31*,107492. doi: 10.1016/j.celrep.2020.03.056.

Bates, D.M., Eiff, C. von, McNamara, P.J., Peters, G., Yeaman, M.R., Bayer, A.S., and Proctor, R.A. (2003). *Staphylococcus aureus menD* and *hemB* mutants are as infective as the parent strains, but the menadione biosynthetic mutant persists within the kidney. J. Infect. Dis. *187*, 1654-61. doi: 10.1086/374642.

Besier, S., Zander, J., Kahl, B.C., Kraiczy, P., Brade, V., and Wichelhaus, T.A. (2009). Hypermutability and antibiotic resistance in thymidinedependent small-colony-variants of *Staphylococcus aureus*. Int. J. Med. Microbiol. *52*, 2183-9. doi: 10.1128/AAC.01395-07.

Blaauboer, S.M., Gabrielle, V.D., and Jin, L. (2014). MPYS/STING-mediated TNF-α, not type I IFN, is essential for the mucosal adjuvant activity of (3′-5′)-cyclic-di-guanosine-monophosphate *in vivo*. J. Immunol. *192*, 492 LP-502.

Blaauboer, S.M., Mansouri, S., Tucker, H.R., Wang, H.L., Gabrielle, V.D., and Jin, L. (2015). The mucosal adjuvant cyclic di-GMP enhances antigen uptake and selectively activates pinocytosis-efficient cells in vivo. Elife. *4*, e06670. doi: 10.7554/eLife.06670.

Brunette, R.L., Young, J.M., Whitley, D.G., Brodsky, I.E., Malik, H.S., and Stetson, D.B. (2012). Extensive evolutionary and functional diversity among mammalian AIM2-like receptors. J. Exp. Med. *209*, 1969-83. doi: 10.1084/jem.20121960.

Burdette, D.L., Monroe, K.M., Sotelo-Troha, K., Iwig, J.S., Eckert, B., Hyodo, M., Hayakawa, Y., and Vance, R.E. (2011). STING is a direct innate immune sensor of cyclic di-GMP. Nature. *478*, 515-8. doi: 10.1038/nature10429.

Chatterjee, I., Kriegeskorte, A., Fischer, A., Deiwick, S., Theimann, N., Proctor, R.A., Peters, G., Herrmann, M., and Kahl, B.C. (2008). *In vivo* mutations of thymidylate synthase (Encoded by *thyA*) are responsible for thymidine dependency in clinical small-colony variants of *Staphylococcus aureus*. J. Bacteriol. *190*, 834-42. doi: 10.1128/JB.00912-07.

Chen, H., Sun, H., You, F., Sun, W., Zhou, X., Chen, L., Yang, J., Wang, Y., Tang, H., Guan, Y., et al. (2011). Activation of STAT6 by STING is critical for antiviral innate immunity. Cell. *147*, 436-46. doi: 10.1016/j.cell.2011.09.022.

Chen, Q., Sun, L., and Chen, Z.J. (2016). Regulation and function of the cGAS-STING pathway of cytosolic DNA sensing. *Nat. Immunol*. *17*, 1142-9. doi: 10.1038/ni.3558.

Choi, P.H., Sureka, K., Woodward, J.J., and Tong, L. (2015). Molecular basis for the recognition of cyclic-di-AMP by PstA, a PII-like signal transduction protein. Microbiologyopen. *4*, 361-74. doi: 10.1002/mbo3.243.

Corrigan, R.M., Abbott, J.C., Burhenne, H., Kaever, V., and Gründling, A. (2011). C-di-AMP is a new second messenger in *Staphylococcus aureus* with a role in controlling cell size and envelope stress. PLoS Pathog. *7*, e1002217. doi: 10.1371/journal.ppat.1002217.

Davies, B.W., Bogard, R.W., Young, T.S., and Mekalanos, J.J. (2012). Coordinated regulation of accessory genetic elements produces cyclic di-nucleotides for *V. cholerae* virulence. Cell. *149*, 358-70. doi: 10.1016/j.cell.2012.01.053.

Dengler, V., McCallum, N., Kiefer, P., Christen, P., Patrignani, A., Vorholt, J.A., Berger-Bächi, B., and Senn, M.M. (2013). Mutation in the c-di-AMP cyclase DacA affects fitness and resistance of methicillin resistant *Staphylococcus aureus*. PLoS One. *8*, e73512. doi: 10.1371/journal.pone.0073512.

Van Dis, E., Sogi, K.M., Rae, C.S., Sivick, K.E., Surh, N.H., Leong, M.L., Kanne, D.B., Metchette, K., Leong, J.J., Bruml, J.R., et al. (2018). STING-activating adjuvants elicit a Th17 immune response and protect against *Mycobacterium tuberculosis* infection. Cell Rep. *23*, 1435-1447. doi: 10.1016/j.celrep.2018.04.003.

Donaldson, S.H., Bennett, W.D., Zeman, K.L., Knowles, M.R., Tarran, R., and Boucher, R.C. (2006). Mucus clearance and lung function in cystic fibrosis with hypertonic saline. N. Engl. J. Med. *354*, 241-50. doi: 10.1056/NEJMoa043891.

Gaidt, M.M., Ebert, T.S., Chauhan, D., Ramshorn, K., Pinci, F., Zuber, S., O'Duill, F., Schmid-Burgk, J.L., Hoss, F., Buhmann, R., et al. (2017). The DNA inflammasome in human myeloid cells is initiated by a STING-cell death program upstream of NLRP3. Cell. *171*, 1110-1124.e18. doi: 10.1016/j.cell.2017.09.039.

Gibhardt, J., Hoffmann, G., Turdiev, A., Wang, M., Lee, V.T., and Commichau, F.M. (2019). C-di-AMP assists osmoadaptation by regulating the *Listeria monocytogenes* potassium transporters KimA and KtrCD. J. Biol. Chem. *294*, 16020-16033. doi: 10.1074/jbc.RA119.010046.

Gui, X., Yang, H., Li, T., Tan, X., Shi, P., Li, M., Du, F., and Chen, Z.J. (2019). Autophagy induction via STING trafficking is a primordial function of the cGAS pathway. Nature. *567*, 262-266. doi: 10.1038/s41586-019-1006-9.

Holland, L.M., O'Donnell, S.T., Ryjenkov, D.A., Gomelsky, L., Slater, S.R., Fey, P.D., Gomelsky, M., and O'Gara, J.P. (2008). A staphylococcal GGDEF domain protein regulates biofilm formation independently of cyclic dimeric GMP. J. Bacteriol. *190*, 5178-89. doi: 10.1128/JB.00375-08.

Huynh, T.A.N., Luo, S., Pensinger, D., Sauer, J.D., Tong, L., and Woodward, J.J. (2015). An HD-domain phosphodiesterase mediates cooperative hydrolysis of c-di-AMP to affect bacterial growth and virulence. Proc. Natl. Acad. Sci. U. S. A. *112*, E747-56. doi: 10.1073/pnas.1416485112.

Huynh, T.A.N., Choi, P.H., Sureka, K., Ledvina, H.E., Campillo, J., Tong, L., and Woodward, J.J. (2016). Cyclic di-AMP targets the cystathionine beta-synthase domain of the osmolyte transporter OpuC. Mol. Microbiol. *102*, 233-243. doi: 10.1111/mmi.13456.

Ishida, Y., Kimura, A., Kondo, T., Hayashi, T., Ueno, M., Takakura, N., Matsushima, K., and Mukaida, N. (2007). Essential roles of the CC chemokine ligand 3-CC chemokine receptor 5 axis in bleomycin-induced

pulmonary fibrosis through regulation of macrophage and fibrocyte infiltration. Am. J. Pathol. *170*, 843-54. doi: 10.2353/ajpath.2007.051213.

Ishikawa, H., and Barber, G.N. (2008). STING is an endoplasmic reticulum adaptor that facilitates innate immune signalling. Nature. *455*, 674-8. doi: 10.1038/nature07317.

Kahl, B.C., Belling, G., Reichelt, R., Herrmann, M., Proctor, R.A., and Peters, G. (2003). Thymidine-dependent small-colony variants of *Staphylococcus aureus* exhibit gross morphological and ultrastructural changes consistent with impaired cell separation. J. Clin. Microbiol. *41*, 410-3. doi: 10.1128/jcm.41.1.410-413.2003.

Kriegeskorte, A., Block, D., Drescher, M., Windmüller, N., Mellmann, A., Baum, C., Neumann, C., Lorè, N.I., Bragonzi, A., Liebau, E., et al. (2014). Inactivation of thyA in Staphylococcus aureus attenuates virulence and has a strong impact on metabolism and virulence gene expression. MBio.

Kriegeskorte, A., Lorè, N.I., Bragonzi, A., Riva, C., Kelkenberg, M., Becker, K., Proctor, R.A., Peters, G., and Kahl, B.C. (2015). Thymidine-dependent *Staphylococcus aureus* small-colony variants are induced by trimethoprim-sulfamethoxazole (SXT) and have increased fitness during SXT challenge. Antimicrob. Agents Chemother. *59*, 7265-72. doi: 10.1128/AAC.00742-15.

Liu, Y., Jesus, A.A., Marrero, B., Yang, D., Ramsey, S.E., Montealegre Sanchez, G.A., Tenbrock, K., Wittkowski, H., Jones, O.Y., Kuehn, H.S., et al. (2014). Activated STING in a vascular and pulmonary syndrome. N. Engl. J. Med. *371*, 507-518. doi: 10.1056/NEJMoa1312625.

Luksch, H., Stinson, W.A., Platt, D.J., Qian, W., Kalugotla, G., Miner, C.A., Bennion, B.G., Gerbaulet, A., Rösen-Wolff, A., and Miner, J.J. (2019). STING-associated lung disease in mice relies on T cells but not type I interferon. J. Allergy Clin. Immunol. *144*, 254-266.e8. doi: 10.1016/j.jaci.2019.01.044.

Mahmoud, L., Abdulkarim, A.S., Kutbi, S., Moghrabi, W., Altwijri, S., Khabar, K.S.A., and Hitti, E.G. (2019). Post-transcriptional inflammatory response to intracellular bacterial c-di-AMP. Front. Immunol. 10, *3050*. doi: 10.3389/fimmu.2019.03050.

McFarland, A.P., Luo, S., Ahmed-Qadri, F., Zuck, M., Thayer, E.F., Goo, Y.A., Hybiske, K., Tong, L., and Woodward, J.J. (2017). Sensing of bacterial cyclic dinucleotides by the oxidoreductase RECON promotes NF-κB activation and shapes a proinflammatory antibacterial state. Immunity. *46*, 433-445. doi: 10.1016/j.immuni.2017.02.014.

McGuinness, W.A., Kobayashi, S.D., and DeLeo, F.R. (2016). Evasion of neutrophil killing by Staphylococcus aureus. Pathogens. *5*, 32. doi: 10.3390/pathogens5010032.

McWhirter, S.M., Barbalat, R., Monroe, K.M., Fontana, M.F., Hyodo, M., Joncker, N.T., Ishii, K.J., Akira, S., Colonna, M., Chen, Z.J., et al. (2009). A host type I interferon response is induced by cytosolic sensing of the bacterial second messenger cyclic-di-GMP. J. Exp. Med. *206*, 1899-911. doi: 10.1084/jem.20082874.

Monk, I.R., Shah, I.M., Xu, M., Tan, M.W., and Foster, T.J. (2012). Transforming the untransformable: application of direct transformation to manipulate genetically *Staphylococcus aureus* and *Staphylococcus epidermidis*. MBio. *3*, e00277-11. doi: 10.1128/mBio.00277-11.

Moretti, J., Roy, S., Bozec, D., Martinez, J., Chapman, J.R., Ueberheide, B., Lamming, D.W., Chen, Z.J., Horng, T., Yeretssian, G., et al. (2017). STING senses microbial viability to orchestrate stress-mediated autophagy of the endoplasmic reticulum. Cell. *171*, 809-823.e13. doi: 10.1016/j.cell.2017.09.034.

Moscoso, J.A., Schramke, H., Zhang, Y., Tosi, T., Dehbi, A., Jung, K., and Gründling, A. (2016). Binding of cyclic di-AMP to the *Staphylococcus aureus* sensor kinase KdpD occurs via the universal stress protein domain and downregulates the expression of the Kdp potassium transporter. J. Bacteriol. *198*, 98-110. doi: 10.1128/JB.00480-15.

Motwani, M., Pawaria, S., Bernier, J., Moses, S., Henry, K., Fang, T., Burkly, L., Marshak-Rothstein, A.,

and Fitzgerald, K.A. (2019). Hierarchy of clinical manifestations in SAVI N153S and V154M mouse models. Proc. Natl. Acad. Sci. U. S. A. *116*, 7941-7950. doi: 10.1073/pnas.1818281116.

Müller, M., Hopfner, K.P., and Witte, G. (2015). C-di-AMP recognition by *Staphylococcus aureus* PstA. *FEBS Lett*. 589, 45-51. doi: 10.1016/j.febslet.2014.11.022.

Oppenheimer-Shaanan, Y., Wexselblatt, E., Katzhendler, J., Yavin, E., and Ben-Yehuda, S. (2011). C-di-AMP reports DNA integrity during sporulation in *Bacillus subtilis*. EMBO Rep. *12*, 594-601. doi: 10.1038/embor.2011.77.

Porto, B.N., and Stein, R.T. (2016). Neutrophil extracellular traps in pulmonary diseases: Too much of a good thing? Front. Immunol. *7*, 311. doi: 10.3389/fimmu.2016.00311. eCollection 2016.

Proctor, R.A., von Eiff, C., Kahl, B.C., Becker, K., McNamara, P., Herrmann, M., and Peters, G. (2006). Small colony variants: a pathogenic form of bacteria that facilitates persistent and recurrent infections. Nat. Rev. Microbiol. *4*, 295-305. doi: 10.1038/nrmicro1384.

Reeves, E.P., Molloy, K., Pohl, K., and McElvaney, N.G. (2012). Hypertonic saline in treatment of pulmonary disease in cystic fibrosis. Sci. World J. *2012*, 465230. doi: 10.1100/2012/465230.

Registry, C.F.F.P. (2018). 2017 Annual Data Report. https://www.cff.org/Research/Researcher-Resources/Patient-Registry/2018-Patient-Registry-Annual-Data-Report.pdf

Sauer, J.-D.D., Witte, C.E., Zemansky, J., Hanson, B., Lauer, P., and Portnoy, D.A. (2010). *Listeria monocytogenes* triggers AIM2-mediated pyroptosis upon infrequent bacteriolysis in the macrophage cytosol. Cell Host Microbe. *7*, 412-9. doi: 10.1016/j.chom.2010.04.004.

Schuster, C.F., Bellows, L.E., Tosi, T., Campeotto, I., Corrigan, R.M., Freemont, P., and Gründling, A. (2016). The second messenger c-di-AMP inhibits the osmolyte uptake system OpuC in *Staphylococcus aureus*. Sci. Signal. *9*, ra81. doi: 10.1126/scisignal.aaf7279.

Smith, S.M., Wunder, M.B., Norris, D.A., and Shellman, Y.G. (2011). A simple protocol for using a LDH-Based cytotoxicity assay to assess the effects of death and growth inhibition at the same time. PLoS One. *6*, e26908. doi: 10.1371/journal.pone.0026908.

Sun, L., Wu, J., Du, F., Chen, X., and Chen, Z.J. (2013). Cyclic GMP-AMP synthase is a cytosolic DNA sensor that activates the type I interferon pathway. Science. *339*, 786-91. doi: 10.1126/science.1232458.

Sureka, K., Choi, P.H., Precit, M., Delince, M., Pensinger, D.A., Huynh, T.A.N., Jurado, A.R., Goo, Y.A., Sadilek, M., Iavarone, A.T., et al. (2014). The cyclic dinucleotide c-di-AMP is an allosteric regulator of metabolic enzyme function. Cell. *158*, 1389-1401. doi: 10.1016/j.cell.2014.07.046.

Suwantarat, N., Rubin, M., Bryan, L., Tekle, T., Boyle, M.P., Carroll, K.C., and Jennings, M.T. (2018). Frequency of small-colony variants and antimicrobial susceptibility of methicillin-resistant *Staphylococcus aureus* in cystic fibrosis patients. Diagn. Microbiol. Infect. Dis. *90*, 296-299. doi: 10.1016/j.diagmicrobio.2017.11.012.

Topp, S., Reynoso, C.M.K., Seeliger, J.C., Goldlust, I.S., Desai, S.K., Murat, D., Shen, A., Puri, A.W., Komeili, A., Bertozzi, C.R., et al. (2010). Synthetic riboswitches that induce gene expression in diverse bacterial species. Appl. Environ. Microbiol. *76*, 7881-4. doi: 10.1128/AEM.01537-10.

Turner, M.S., Vu, T.N.M., Marcellin, E., Liang, Z.-X., and Pham, H.T. (2020). Osmoregulation via Cyclic di-AMP Signaling BT - Microbial Cyclic Di-Nucleotide Signaling. S.-H. Chou, N. Guiliani, V.T. Lee, and U. Römling, eds. (Cham: Springer International Publishing), pp. 177-189.

Warner, J.D., Irizarry-Caro, R.A., Bennion, B.G., Ai, T.L., Smith, A.M., Miner, C.A., Sakai, T., Gonugunta, V.K., Wu, J., Platt, D.J., et al. (2017). STING-associated vasculopathy develops independently of IRF3 in mice. J. Exp. Med. *214*, 3279-3292. doi: 10.1084/jem.20171351.

Weischenfeldt, J., and Porse, B. (2008). Bone marrow-derived macrophages (BMM): Isolation and applications. Cold Spring Harb. Protoc. *2008*, pdb.prot5080. doi: 10.1101/pdb.prot5080.

Whiteley, A.T., Eaglesham, J.B., de Oliveira Mann, C.C., Morehouse, B.R., Lowey, B., Nieminen, E.A., Danilchanka, O., King, D.S., Lee, A.S.Y., Mekalanos, J.J., et al. (2019). Bacterial cGAS-like enzymes synthesize diverse nucleotide signals. Nature. *567*, 194-199. doi: 10.1038/s41586-019-0953-5.

Whitney, J.C., Peterson, S.B., Kim, J., Pazos, M., Verster, A.J., Radey, M.C., Kulasekara, H.D., Ching, M.Q., Bullen, N.P., Bryant, D., et al. (2017). A broadly distributed toxin family mediates contact-dependent antagonism between gram-positive bacteria. Elife. *6*, e26938. doi: 10.7554/eLife.26938.

Witte, C.E., Whiteley, A.T., Burke, T.P., Sauer, J.D., Portnoy, D.A., and Woodward, J.J. (2013). Cyclic di-AMP is critical for *Listeria monocytogenes* growth, cell wall homeostasis, and establishment of infection. MBio. *4*, e00282-13. doi: 10.1128/mBio.00282-13.infection. MBio.

Wolter, D.J., Emerson, J.C., McNamara, S., Buccat, A.M., Qin, X., Cochrane, E., Houston, L.S., Rogers, G.B., Marsh, P., Prehar, K., et al. (2013). *Staphylococcus aureus* small-colony variants are independently associated with worse lung disease in children with cystic fibrosis. Clin. Infect. Dis. *57*, 384-91. doi: 10.1093/cid/cit270.

Wolter, D.J., Onchiri, F.M., Emerson, J., Precit, M.R., Lee, M., McNamara, S., Nay, L., Blackledge, M., Uluer, A., Orenstein, D.M., et al. (2019). Prevalence and clinical associations of *Staphylococcus aureus* small-colony variant respiratory infection in children with cystic fibrosis (SCVSA): a multicentre, observational study. Lancet Respir. Med. *7*, 1027-1038. doi: 10.1016/S2213-2600(19)30365-0.

Woodward, J.J., Lavarone, A.T., and Portnoy, D.A. (2010). C-di-AMP secreted by intracellular Listeria monocytogenes activates a host type I interferon response. Science. *328*, 1703-5. doi: 10.1126/science.1189801.

Wu, J., Sun, L., Chen, X., Du, F., Shi, H., Chen, C., and Chen, Z.J. (2013). Cyclic GMP-AMP is an endogenous second messenger in innate immune signaling by cytosolic DNA. Science. *339*, 826-30. doi: 10.1126/science.1229963.

Yagci, S., Hascelik, G., Dogru, D., Ozcelik, U., and Sener, B. (2013). Prevalence and genetic diversity of *Staphylococcus aureus* small-colony variants in cystic fibrosis patients. Clin. Microbiol. Infect. *19*, 77-84. doi: 10.1111/j.1469-0691.2011.03742.x.

Yang, X., Walton, W., Cook, D.N., Hua, X., Tilley, S., Haskell, C.A., Horuk, R., Blackstock, A.W., and Kirby, S.L. (2011). The chemokine, CCL3, and its receptor, CCR1, mediate thoracic radiation-induced pulmonary fibrosis. Am. J. Respir. Cell Mol. Biol. *45*, 127-35. doi: 10.1165/rcmb.2010-0265OC.

Yi, G., Brendel, V.P., Shu, C., Li, P., Palanathan, S., and Cheng Kao, C. (2013). Single nucleotide polymorphisms of human STING can affect innate immune response to cyclic dinucleotides. PLoS One. *8*, e77846. doi: 10.1371/journal.pone.0077846.

Zander, J., Besier, S., Saum, S.H., Dehghani, F., Loitsch, S., Brade, V., and Wichelhaus, T.A. (2008). Influence of dTMP on the phenotypic appearance and intracellular persistence of *Staphylococcus aureus*. Infect. Immun. *76*, 1333-9. doi: 10.1128/IAI.01075-07.

Zander, J., Besier, S., Faetke, S., Saum, S.H., Müller, V., and Wichelhaus, T.A. (2010). Antimicrobial activities of trimethoprim/sulfamethoxazole, 5-iodo-2′-deoxyuridine and rifampicin against *Staphylococcus aureus*. Int. J. Antimicrob. Agents. *36*, 562-5. doi: 10.1016/j.ijantimicag.2010.08.007.

Zaver, S.A., and Woodward, J.J. (2020). Cyclic dinucleotides at the forefront of innate immunity. Curr. Opin. Cell Biol. *63*, 49-56. doi: 10.1016/j.ceb.2019.12.004.

Zeden, M.S., Schuster, C.F., Bowman, L., Zhong, Q., Williams, H.D., and Gründling, A. (2018). Cyclic di-adenosine monophosphate (c-di-AMP) is required for osmotic regulation in *Staphylococcus aureus* but

dispensable for viability in anaerobic conditions. J. Biol. Chem. *293*, 3180-3200. doi: 10.1074/jbc.M117.818716.

Zhang, H., Zeng, L., Xie, M., Liu, J., Zhou, B., Wu, R., Cao, L., Kroemer, G., Wang, H., Billiar, T.R., et al. (2020). TMEM173 drives lethal coagulation in sepsis. Cell Host Microbe. *27*, 556-570.e6. doi: 10.1016/j.chom.2020.02.004.

Zhang, X., Shi, H., Wu, J., Zhang, X., Sun, L., Chen, C., and Chen, Z.J. (2013). Cyclic GMP-AMP containing mixed Phosphodiester linkages is an endogenous high-affinity ligand for STING. Mol. Cell. *51*, 226-35. doi: 10.1016/j.molcel.2013.05.022.

Main Figure

Figure 1

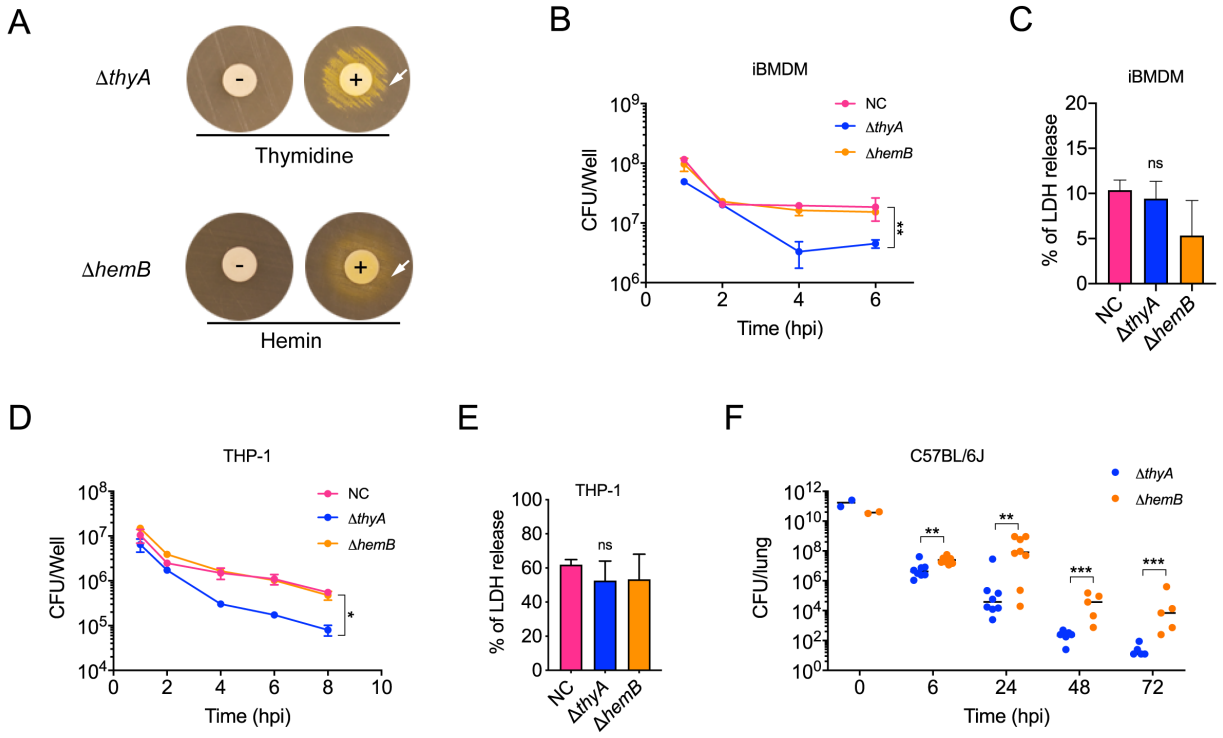

Figure 2

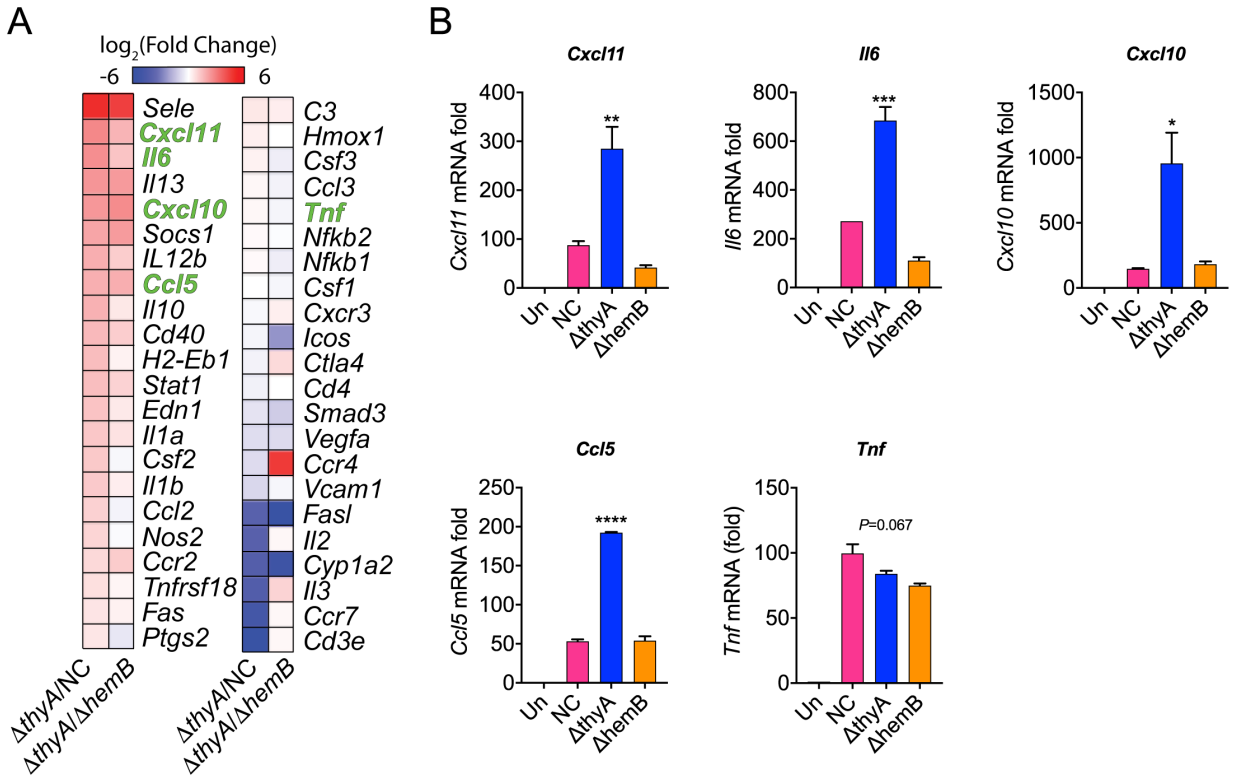
A
log2(Fold Change)
-6
6
Sele
Cxcl11
Il6
Il13
Cxcl10
Socs1
IL12b
Ccl5
Il10
Cd40
H2-Eb1
Stat1
Edn1
Il1a
Csf2
Il1b
Ccl2
Nos2
Ccr2
Tnfrsf18
Fas
Ptgs2
C3
Hmox1
Csf3
Ccl3
Tnf
Nfkb2
Nfkb1
Csf1
Cxcr3
Icos
Ctla4
Cd4
Smad3
Vegfa
Ccr4
Vcam1
Fasl
Il2
Cyp1a2
Il3
Ccr7
Cd3e
ΔthyA/NC
ΔthyA/ΔhemB
ΔthyA/NC
ΔthyA/ΔhemB
B
Cxcl11
Cxcl11 mRNA fold
400
300
200
100
0
**
Un
NC
ΔthyA
ΔhemB
Il6
Il6 mRNA fold
800
600
400
200
0
***
Cxcl10
Cxcl10 mRNA fold
1500
1000
500
0
*
Ccl5
Ccl5 mRNA fold
250
200
150
100
50
0
****
Tnf
Tnf mRNA (fold)
150
100
50
0
P=0.067

Figure 3

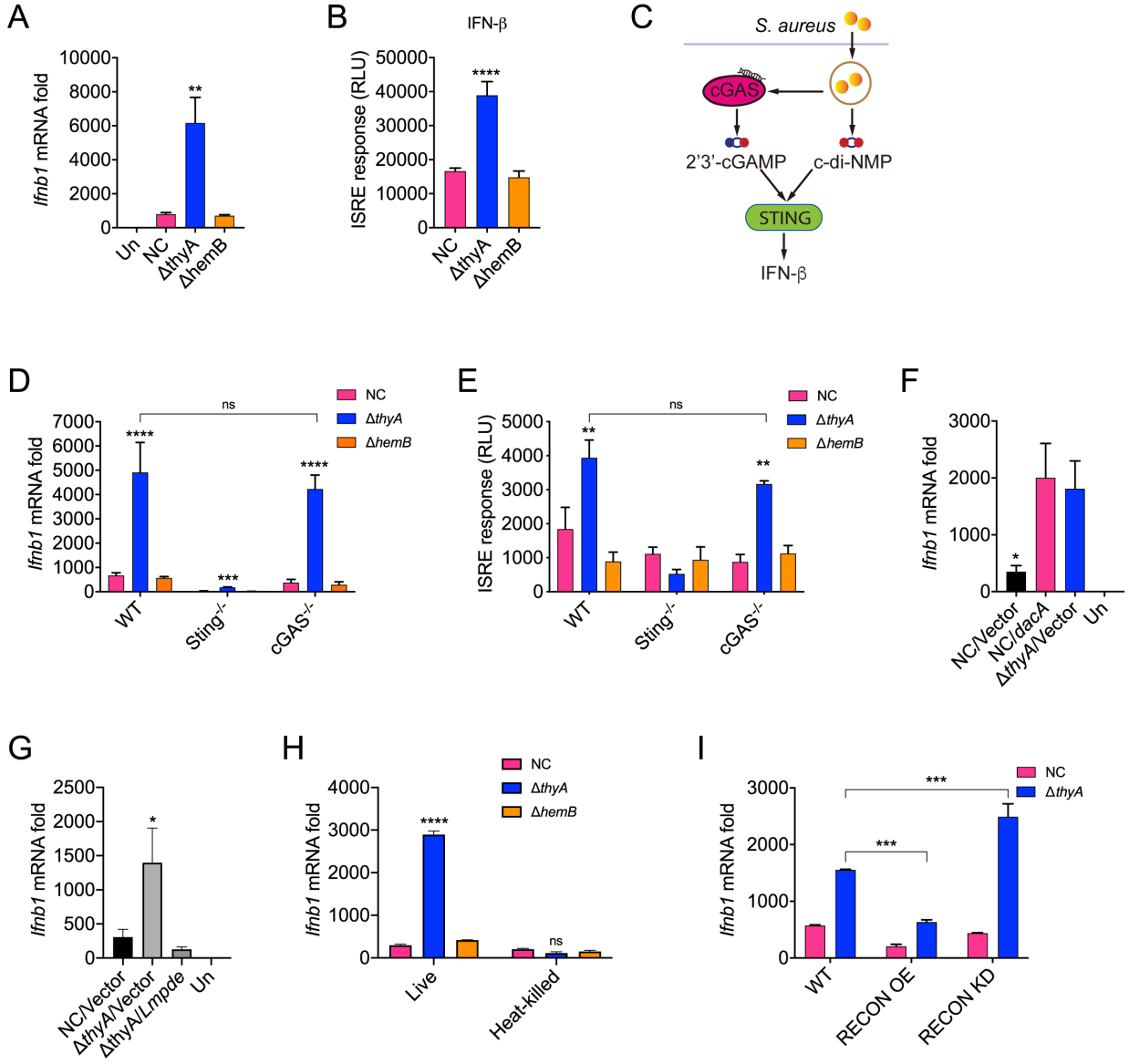
A
Ifnb1 mRNA fold
10000
8000
6000
4000
2000
0
**
Un
NC
ΔthyA
ΔhemB
B
IFN-β
ISRE response (RLU)
50000
40000
30000
20000
10000
0
****
NC
ΔthyA
ΔhemB
C
S. aureus
cGAS
2'3'-cGAMP
c-di-NMP
STING
IFN-β
D
Ifnb1 mRNA fold
7000
6000
5000
4000
3000
2000
1000
0
ns
****
***
****
NC
ΔthyA
ΔhemB
WT
Sting-/-
cGAS-/-
E
ISRE response (RLU)
5000
4000
3000
2000
1000
0
ns
**
**
NC
ΔthyA
ΔhemB
WT
Sting-/-
cGAS-/-
F
Ifnb1 mRNA fold
3000
2000
1000
0
*
NC/Vector
NC/dacA
ΔthyA/Vector
Un
G
Ifnb1 mRNA fold
2500
2000
1500
1000
500
0
*
NC/Vector
ΔthyA/Vector
ΔthyA/Lmpde
Un
H
Ifnb1 mRNA fold
4000
3000
2000
1000
0
****
ns
NC
ΔthyA
ΔhemB
Live
Heat-killed
I
Ifnb1 mRNA fold
3000
2000
1000
0
***
***
NC
ΔthyA
WT
RECON OE
RECON KD

Figure 4

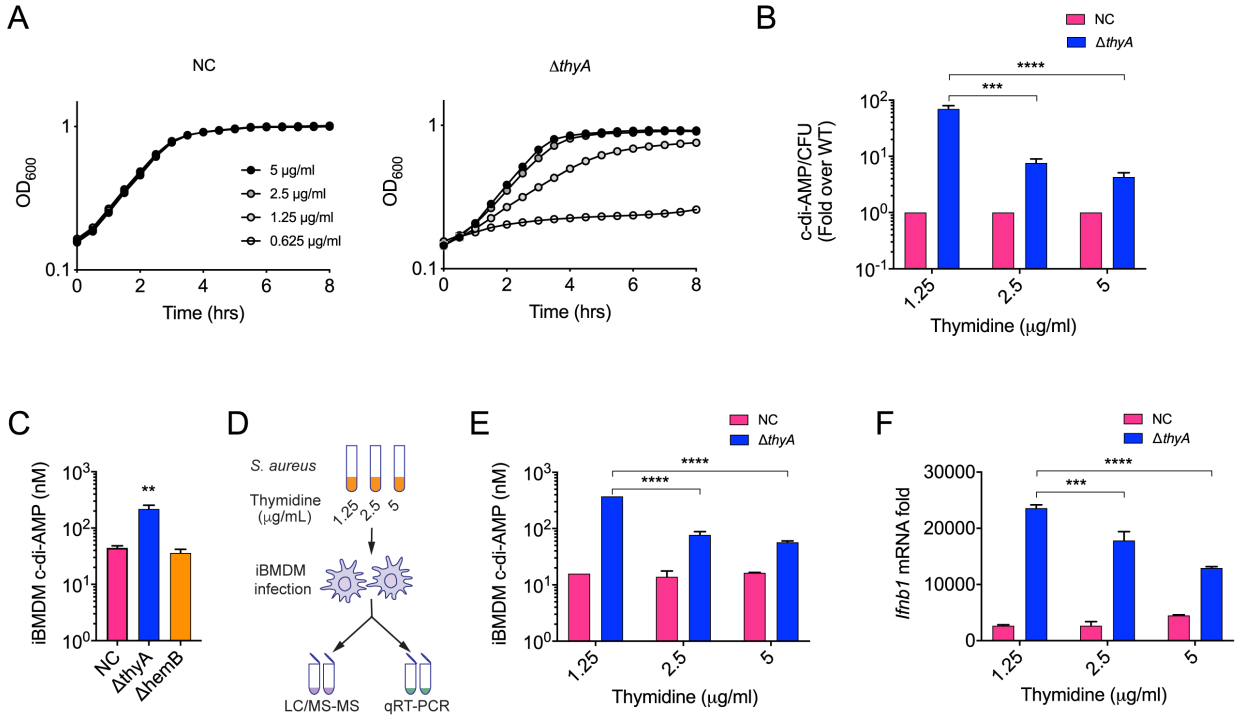
A
NC
ΔthyA
OD600
Time (hrs)
5 μg/ml
2.5 μg/ml
1.25 μg/ml
0.625 μg/ml
B
NC
ΔthyA
c-di-AMP/CFU (Fold over WT)
Thymidine (μg/ml)
C
iBMDM c-di-AMP (nM)
NC
ΔthyA
ΔhemB
D
S. aureus
Thymidine (μg/mL)
iBMDM infection
LC/MS-MS
qRT-PCR
E
iBMDM c-di-AMP (nM)
Thymidine (μg/ml)
F
Ifnb1 mRNA fold
Thymidine (μg/ml)

Figure 5

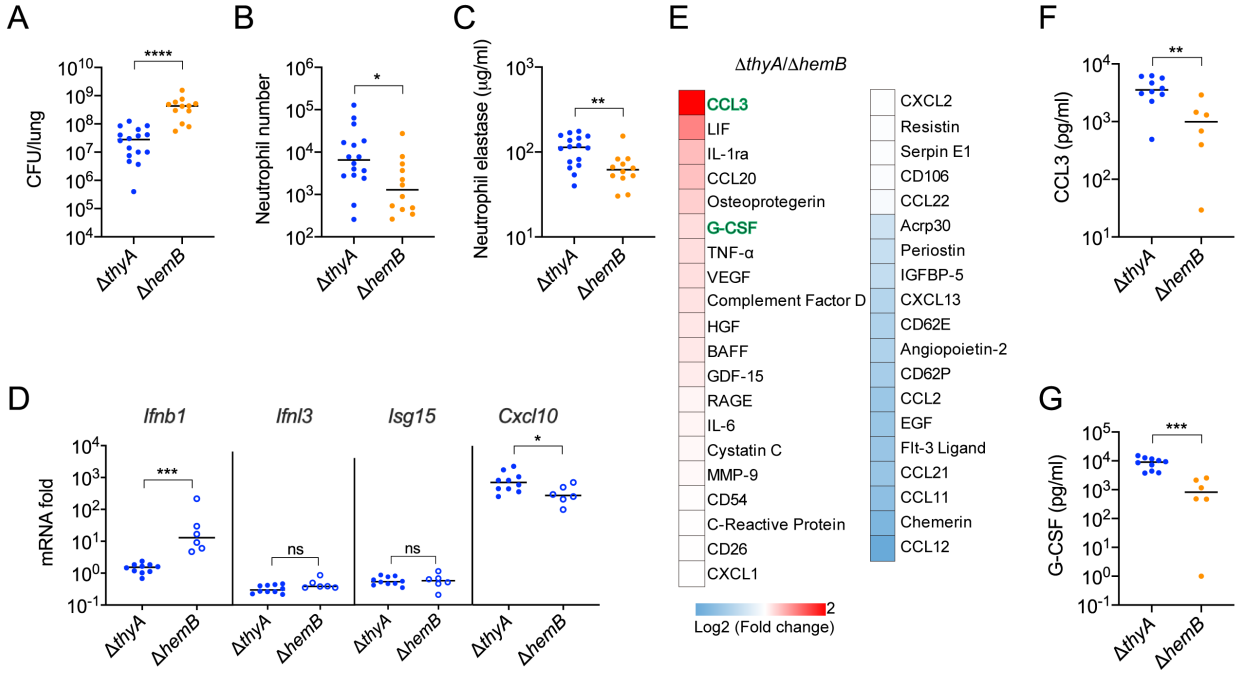
A
CFU/lung
****
ΔthyA
ΔhemB
B
Neutrophil number
*
C
Neutrophil elastase (μg/ml)
**
D
Ifnb1
Ifnl3
Isg15
Cxcl10
mRNA fold
***
ns
ns
*
E
ΔthyA/ΔhemB
CCL3
LIF
IL-1ra
CCL20
Osteoprotegerin
G-CSF
TNF-α
VEGF
Complement Factor D
HGF
BAFF
GDF-15
RAGE
IL-6
Cystatin C
MMP-9
CD54
C-Reactive Protein
CD26
CXCL1
CXCL2
Resistin
Serpin E1
CD106
CCL22
Acrp30
Periostin
IGFBP-5
CXCL13
CD62E
Angiopoietin-2
CD62P
CCL2
EGF
Flt-3 Ligand
CCL21
CCL11
Chemerin
CCL12
2
Log2 (Fold change)
F
CCL3 (pg/ml)
**
G
G-CSF (pg/ml)
***

Figure 6

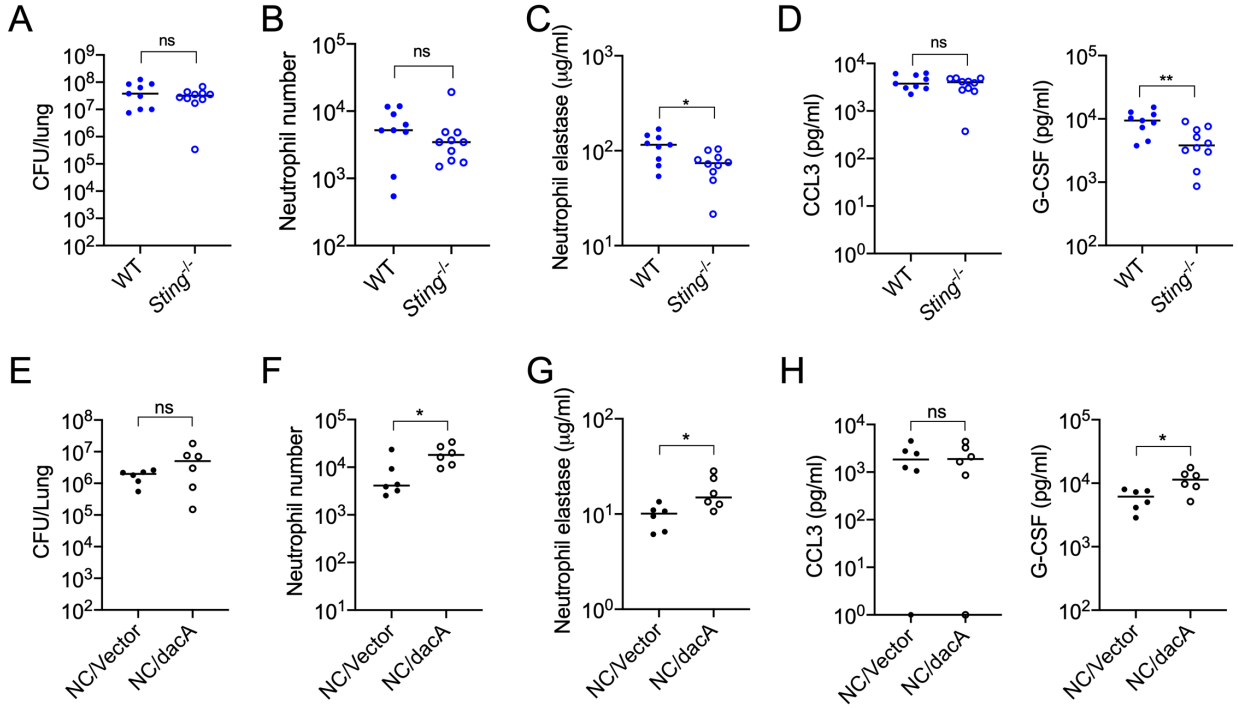
A
CFU/lung
ns
WT
Sting-/-
B
Neutrophil number
ns
WT
Sting-/-
C
Neutrophil elastase (μg/ml)
*
WT
Sting-/-
D
CCL3 (pg/ml)
ns
WT
Sting-/-
G-CSF (pg/ml)
**
WT
Sting-/-
E
CFU/Lung
ns
NC/Vector
NC/dacA
F
Neutrophil number
*
NC/Vector
NC/dacA
G
Neutrophil elastase (μg/ml)
*
NC/Vector
NC/dacA
H
CCL3 (pg/ml)
ns
NC/Vector
NC/dacA
G-CSF (pg/ml)
*
NC/Vector
NC/dacA

Figure 7

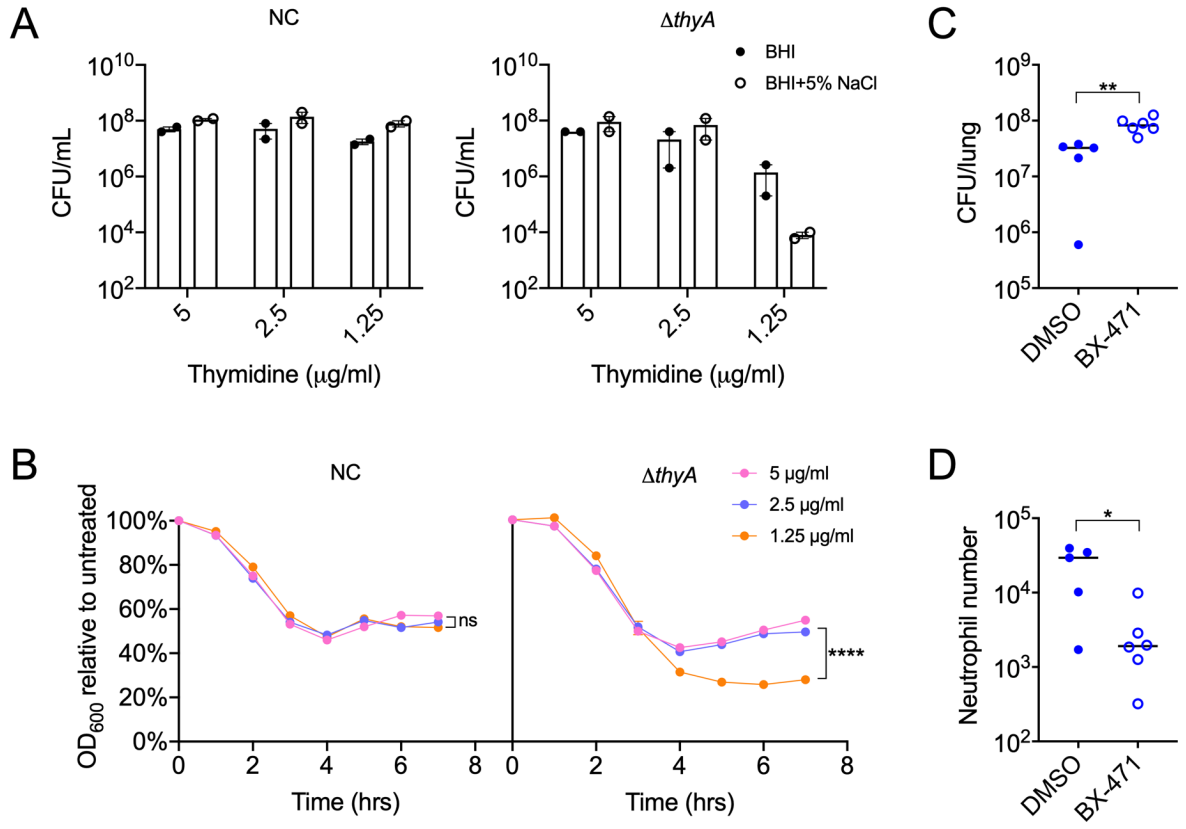
A
NC
ΔthyA
BHI
BHI+5% NaCl
CFU/mL
Thymidine (μg/ml)
5
2.5
1.25
C
CFU/lung
DMSO
BX-471
**
B
NC
ΔthyA
5 μg/ml
2.5 μg/ml
1.25 μg/ml
OD600 relative to untreated
Time (hrs)
ns
****
D
Neutrophil number
*

KEY RESOURCES TABLE

REAGENT or RESOURCE	SOURCE	IDENTIFIER
Antibodies		
Brilliant Violet 421 anti-mouse Ly-6G	BioLegend	Cat# 101319; RRID: AB_1574973
PE/Dazzle 594 anti-mouse/human CD11b	BioLegend	Cat# 101319; RRID: AB_1574973
PerCP/Cyanine5.5 anti-mouse CD45	BioLegend	Cat# 103131; RRID: AB_893344
PE anti-mouse F4/80	BioLegend	Cat# 123109; RRID: AB_893498
TruStain FcX™ PLUS anti-mouse CD16/32	BioLegend	Cat# 101319; RRID: AB_1574973
Bacterial and Virus Strains		
Staphylococcus aureus Newman	Laboratory stock	N/A
Staphylococcus aureus Newman Δ*thyA*	This paper	N/A
Staphylococcus aureus Newman Δ*hemB*	This paper	N/A
Staphylococcus aureus Rn4220	Laboratory stock	N/A
Escherichia coli XL1-blue	Agilent Technologies	Cat# 50-125-058
Escherichia coli DH10B	(Monk et al., 2012)	N/A
Chemicals, Peptides, and Recombinant Proteins		
BX-471	Cayman	Cat# 18503
c-di-AMP	Invivogen	Cat# tlrl-nacda
^{3}H-c-di-AMP	This paper	N/A
MeOSuc-Ala-Ala-Pro-Val-AMC	Cayman	Cat# 14907
Lipofectamine 2000	Thermo Fisher	Cat# 11668027
Elastase from porcine pancreas	Sigma	SKU# E7885
Reagent or Resource		
TaqMan Gene Expression Master Mix	Applied Biosystems	Cat# 43-695-10
NucleoSpin RNA Plus Kit	Clontech	Cat# 740984.50
iScript cDNA Synthesis Kit	Bio-Rad	Cat# 1708891
Mouse *Ccl3* TaqMan probe	Thermo Fisher	Assay ID: Mm00441259_g1
Mouse *Hprt* TaqMan probe	Thermo Fisher	Assay ID: Mm03024075_m1
Mouse *Ifnb1* TaqMan probe	Thermo Fisher	Assay ID: Mm00439552_s1
Mouse *Isg15* TaqMan probe	Thermo Fisher	Assay ID: Mm01705338_s1
Mouse *Ifnl3* TaqMan probe	Thermo Fisher	Assay ID: Mm00663660_g1
Mouse *Cxcl10* TaqMan probe	Thermo Fisher	Assay ID: Mm00445235_m1
TaqMan Array Mouse Immune Panel	Applied Biosystems	Cat# 4367786
Zombie Green™ Fixable Viability Kit	BioLegend	Cat# 423111
Red Cell Lysis Buffer	BioLegend	Cat# 420301
Cell Staining Buffer	BioLegend	Cat# 420201
LDH-Glo Cytotoxicity Assay	Promega	Cat# J2380
Mouse CCL3/MIP-1 alpha Quantikine ELISA Kit	R&D systems	Cat# MMA00
Mouse G-CSF Quantikine ELISA Kit	R&D systems	Cat# MCS00
Proteome Profiler Mouse XL Cytokine Array	R&D systems	Cat# ARY028
Experimental Models: Cell Lines		
Human: THP-1	ATCC	SKU# 88081201
Murine: J2 immortalized BMDMs	(Sauer et al., 2010)	N/A
Murine: WT, *Tmem173*$^{-/-}$, *cGAS*$^{-/-}$ primary BMDMs	This paper	N/A
Murine: ISRE-L929 cells	(Woodward et al., 2010)	N/A
Experimental Models: Organisms/Strains		

Mouse: C57BL/6J	The Jackson Laboratory	JAX: 000664
Mouse: C57BL/6J *Tmem173*$^{-/-}$	(Brunette et al., 2012)	N/A
Mouse: C57BL/6J *cGAS*$^{-/-}$	(Brunette et al., 2012)	N/A
Mouse: C57BL/6J *Sting*$^{Gt/Gt}$	The Jackson Laboratory	JAX: 017537
Oligonucleotides		
Oligonucleotides used in *S. aureus* mutant construction	This paper	See Table S1
Oligonucleotides used in construction of *dacA* or *lmpde* overexpression vectors	This paper	See Table S1
Oligonucleotides used in mouse genotyping	This paper	See Table S1
Recombinant DNA		
pIMAY	(Monk et al., 2012)	N/A
pIMAY-derivative plasmids	This paper	N/A
pBAV1K-E*	(Topp et al., 2010)	N/A
pBAV1K-E*-*dacA* expression plasmid	This paper	N/A
pEPSA5	(Whitney et al., 2017)	N/A
pEPSA5-*Lmpde* expression plasmid	This paper	N/A
Software and Algorithms		
Prism 6.0	GraphPad	https://www.graphpad.com/scientific-software/prism/; RRID:SCR_002798
Morpheus	Broad Institute	https://software.broadinstitute.org/morpheus/; RRID:SCR_017386
FlowJo v10.7	FlowJo	https://www.flowjo.com/solutions/flowjo; RRID:SCR_008520
Adobe Photoshop	Adobe	https://www.adobe.com/products/photoshop.html; RRID:SCR_014199
Adobe Illustrator 2019	Adobe	http://www.adobe.com/products/illustrator.html; RRID:SCR_010279
Image studio v5.2	LI-COR Biosciences	https://www.licor.com/bio/image-studio-lite/; RRID:SCR_015795
Other		
Synergy HTX Multi-Mode Reader	BioTek	
Cytek Aurora	Cytek	
Odyssey Fc Imaging System	LI-COR Biosciences	
CFX Connect Real-Time PCR Detection System	Bio-Rad	Cat# 1855200
Tissue-Tearor Homogenizer	BioSpec	Model# 985370-14
ViiA 7 Real-Time PCR System	Applied Biosystems	